

Pseudo-thermalization in driven-dissipative non-Markovian open quantum systems

José Lebreuilly*

INO-CNR BEC Center and Dipartimento di Fisica, Università di Trento, I-38123 Povo, Italy

Alessio Chiocchetta

Institut für Theoretische Physik, Universität zu Köln, D-50937 Cologne, Germany

Iacopo Carusotto

INO-CNR BEC Center and Dipartimento di Fisica, Università di Trento, I-38123 Povo, Italy

We investigate a ‘pseudo thermalization’ effect, where an open quantum system coupled to several non-Markovian reservoirs presents an emergent thermal behaviour in spite of its coupling to a non-equilibrated environment. The thermal behaviour is visible at both static and dynamical levels and the system satisfies the fluctuation-dissipation theorem. Our analysis is focused on the exactly solvable model of a weakly interacting driven-dissipative Bose gas in presence of frequency-dependent particle pumping and losses, and is based on a quantum Langevin theory, which we derive starting from a microscopical quantum optics model. For generic non-Markovian reservoirs, we demonstrate that the emergence of thermal properties occurs in the range of frequencies corresponding to low-energy excitations. For the specific case of non-Markovian baths verifying the Kennard-Stepanov relation, we show that pseudo-thermalization can instead occur at all energy scales. The possible implications regarding the interpretation of thermal laws in exciton-polariton low temperature experiments are discussed. We finally show that the presence of either a saturable pumping or a dispersive environment leads to a breakdown of the pseudo-thermalization effect.

I. INTRODUCTION

Our understanding of the conditions allowing for the emergence of equilibrium features in driven-dissipative quantum systems is still incomplete. The dynamics of open quantum systems is often characterized by the presence of a complex external environment, implementing a wide range of effects such as single particle and many-body losses, pump, dephasing [1, 2], or more exotic dissipative processes [3], which are usually modelled as a series of external reservoirs [4, 5]. Due to the presence of dissipation, in the generic situation an open quantum system is expected to reach after a long enough evolution a steady-state where observables no longer evolve in time [6, 7]. Although it is a widely accepted belief that in presence of a typical non-equilibrated environment the system properties do not necessarily recover those predicted by some thermal model, a quantitative estimation of the deviations between the steady-state and equilibrium predictions often reveals challenging.

Over the last decade, these problematics have become particularly relevant at an experimental level also in the quantum regime, as pioneering works in photonic devices have opened a whole new research direction on the dynamics of non-equilibrium quantum fluids. Signatures of Bose-Einstein distributions, such as the presence of power-law infrared divergencies similar to the Rayleigh-Jeans distribution ($n_k \propto k^{-2}$ for $k \rightarrow 0$), and/or high-energy exponential tails of a Boltzmann type ($n_k \propto \exp[-\beta E_k]$ for $k \rightarrow \infty$), have been observed in several experiments involving photon and exciton-polariton non-equilibrium gases [8–15]. In room temperature

experiments [11–15], the appearance of thermal correlations might be seen as something rather predictable since energy exchange with the thermal environment is occurring much faster than particle losses. Yet, in other classes of low-temperature exciton-polaritons [8, 9] and VCSEL [10] experiments where non-equilibrium effects are expected to be kinetically dominant, the underlying mechanisms leading to the emergence of an effective temperature differing from the one of the apparatus are less clear and subject to controversy [16–18].

From a theoretical point of view, many studies have quantified the distance from equilibrium for photonic systems [16, 19–23] and connections have been drawn between equilibrium and symmetries of the Keldysh action [24, 25]. Works based on renormalization group (RG) methods for non-equilibrium field theories have addressed the long-range and low-energy properties of quantum fluids and the critical properties across a classical [26, 27] or quantum phase transition [28]. In particular, the important role played by the spatial dimensionality in determining whether a driven-dissipative quantum system presents asymptotic thermal properties was pointed out in many studies [26, 29–31]. More recently, the necessity of characterizing the dynamical properties was also pointed out in [32], where it was showed that a driven-dissipative quantum system could present at steady-state equilibrium-like static correlations without verifying the Fluctuation-Dissipation Theorem (FDT) at a dynamical level.

Here we want to push this last statement one step further: we argue that, under specific conditions, an open quantum system can present all the attributes of an equilibrated system both at a static and a dynamic level, verifying thus the FDT theorem, even though its environment is highly non-thermal. In a previous work [33], we unveiled a preliminary result in this direction for a quantum optical model, where we showed that apparent thermalization can be obtained by coupling the system to several non-thermal and non-Markovian

*Electronic address: jose.lebreuilly@unitn.it

baths, which effectively mimic the impact of a single thermal bath. While long-range asymptotic thermal properties had already been predicted to emerge [26, 27] in high enough dimensions in generic interacting non-equilibrium systems, we stress that the effective equilibrium predicted here relies on a different physical mechanism: whenever the Kennard-Stepanov (KS) relation [34, 35] (i.e., a particular form of detailed balance relation) is verified in our model, the system is not able to perceive that the reservoirs are not equilibrated and its steady-state coincides with a thermal state, with both temperature and chemical potential being emergent quantities depending on the various baths spectral properties. We choose to call this effect “*pseudo-thermalization*”.

Following [33], the preliminary concept was deepened in [36], who suggested to engineer more complex reservoirs so to reproduce this mechanism over broader energy scales, and then obtain artificial and controllable temperatures in view of optimizing the performance of quantum annealers. Some hints suggest that the apparent emergence of thermal static properties in low-T exciton-polariton [8, 9] and VCSEL [10] experiments might be related to pseudo-thermalization in some experimental configurations. In the very recent work [37], we suggested to exploit a closely related effect to stabilize photonic Mott Insulating states close to zero temperature.

In both works [33, 36], the formalism was based on a quantum master equation formalism, which allowed to compute the static properties of the steady-state. However, due to the absence of a regression theorem for non-Markovian problems [6, 38], such approach does not allow to access dynamical physical quantities such as multiple time correlators, and in particular is not suited to verify the validity of the fluctuation-dissipation Theorem (FDT) [39]. Moreover, as all predictions were based on very general theoretical arguments, a full validation on an exactly solvable model still remains to provide.

In this paper, we investigate pseudo-thermalization effects for the specific model of a weakly interacting BEC coupled to several non-Markovian reservoirs. In contrast with [33, 36] we develop an alternative analytical approach based on a quantum Langevin formalism which keeps tracks of the bath dynamics and in particular allows to access both static and dynamical properties of the steady state. In this way, we are able not only to demonstrate the presence of thermal signatures at a static level, but also to show that the fluctuation-dissipation theorem is verified at a dynamical level.

This paper is organized as follows: in Sec. II we introduce the general Langevin model and use a Bogoliubov approach to linearize the theory around a mean-field solution, from which we demonstrate numerically the dynamical stability. We also derive a low-energy effective description, allowing to provide exact analytical expressions for the low-momentum Bogoliubov spectrum. In Sec. III, we show that, for baths with arbitrary spectral shape, this model presents low-energy pseudo-thermalization both at a static and dynamical level: we demonstrate at low energies that not only static correlations match with their thermal counterpart, but that the FDT is also verified. Moreover, if the non-thermal baths are suitably chosen to verify the Kennard-Stepanov (KS) relation at all energies, then the system undergoes thermalization at

all energies. In Sec. IV we provide a microscopic derivation of the quantum Langevin model starting from a quantum optical model involving frequency-dependent losses and emitters with a non-trivial distribution of transition frequencies. We also explain how the Kennard-Stepanov relation could be engineered with this model, and how it might be naturally reproduced in some specific exciton-polariton low-T experiments. In Sec. V we give hints on how pseudo-thermalization can be broken and the system be driven out-of-equilibrium by adding saturation and/or non-trivial momentum dependence to the dissipative processes responsible for particle pumping. Conclusions are given in Sec. VI.

II. NON-MARKOVIAN QUANTUM-LANGEVIN EQUATION

In this section we express the dynamics of a driven-dissipative interacting Bose Gas in contact with non-Markovian reservoirs in terms of a quantum Langevin formalism. This model had already been addressed in [33, 37] in a quantum optics context and formulated in terms of a Redfield equation. Focusing on the weakly interacting case, in the BEC regime we study the mean-field solution of this model and use the Bogoliubov theory to study the dynamics of fluctuations. After demonstrating numerically the dynamical stability for a specific choice of the pump and loss spectra, we develop a low-energy effective theory so to access analytically the low-momentum collective modes of the condensate.

A. Model for a driven condensate

Let us consider a bosonic gas in d spatial dimensions, described by the annihilation and creation fields $\hat{\psi}(\mathbf{r})$ and $\hat{\psi}^\dagger(\mathbf{r})$. The evolution in time of these operators is described by the non-Markovian quantum-Langevin equation

$$\frac{\partial \hat{\psi}}{\partial t}(\mathbf{r}, t) = -i \left[\omega_0 - \frac{\nabla^2}{2m} + g \hat{\psi}^\dagger(\mathbf{r}, t) \hat{\psi}(\mathbf{r}, t) \right] \hat{\psi}(\mathbf{r}, t) + \int_{t'} \Gamma(t') \hat{\psi}(\mathbf{r}, t - t') + \hat{\xi}(\mathbf{r}, t), \quad (2.1)$$

where $\int_{t'} \equiv \int_{-\infty}^{+\infty} dt'$, while ω_0 is the bare cavity frequency, m is the bosonic mass, $g > 0$ is the strength of the repulsive contact interaction, Γ is a memory kernel and $\hat{\xi}(\mathbf{r}, t)$ a zero-mean Gaussian quantum noise operator. Equation (2.1) resembles the Heisenberg equation for the motion of the operator $\hat{\psi}$ for an isolated interacting Bose gas. However, the dynamics described by Eq. (2.1) does not conserve energy and number of particles. Namely, the memory kernel $\Gamma(t')$ and quantum noise $\hat{\xi}(t)$ terms model altogether the effect of non-Markovian particle losses and pumping (i.e., injection) dissipative processes, whose respective strength is quantified by the frequency-dependent power spectra $\mathcal{S}_l(\omega)$ and $\mathcal{S}_p(\omega)$.

Within the Langevin formalism, the correlations of the

noise operators $\hat{\psi}(\mathbf{r}, t)$, $\hat{\psi}^\dagger(\mathbf{r}, t)$ can be written as

$$\langle \hat{\xi}(t) \hat{\xi}^\dagger(t') \rangle = \int_{\omega} S_l(\omega) e^{-i\omega(t-t')} \quad (2.2a)$$

$$\langle \hat{\xi}^\dagger(t) \hat{\xi}(t') \rangle = \int_{\omega} S_p(\omega) e^{i\omega(t-t')}, \quad (2.2b)$$

with $\int_{\omega} \equiv \int_{-\infty}^{+\infty} d\omega/(2\pi)$. Likewise, Γ is expressed as

$$\Gamma(t) = \theta(t) \int_{\omega} [S_p(\omega) - S_l(\omega)] e^{-i\omega t}. \quad (2.3)$$

The Heaviside function $\theta(t)$ in Eq. (2.3) is needed in order to ensure causality: as a result, its presence implies the Kramers-Kronig relations between the real and imaginary parts of the Fourier transform $\Gamma(\omega) = \int_t e^{i\omega t} \Gamma(t)$, which can thus be written as

$$\text{Re} [\Gamma(\omega)] = \frac{1}{2} [S_p(\omega) - S_l(\omega)], \quad (2.4a)$$

$$\text{Im} [\Gamma(\omega)] = \text{PV} \int_{\omega'} \frac{S_p(\omega') - S_l(\omega')}{\omega - \omega'}. \quad (2.4b)$$

The power spectra $S_p(\omega)$ and $S_l(\omega)$ are assumed to be smooth functions of the frequency ω . In the following, we will restrict to the case in which there exists a range of frequencies $\omega_1 < \omega < \omega_2$ such that $S_p(\omega) > S_l(\omega)$ (“amplifying” region), and that $S_p(\omega) < S_l(\omega)$ outside this interval (“lossy” region). Accordingly, losses are perfectly balanced by pumping at the boundary of this interval, i.e., $S_p(\omega_{1,2}) = S_l(\omega_{1,2})$. We also define $\Delta_{\text{diss}} = \min(\text{FWHM}(S_l), \text{FWHM}(S_p))$ as the minimum of the full width at half maximum of the power spectra $S_l(\omega)$ and $S_p(\omega)$. It represents a characteristic frequency scale over which these power spectra change value and quantifies the non-Markovianity of the dynamics.

We stress that the loss and pump power spectra $S_l(\omega)$ and $S_p(\omega)$ arise from the contact of the system with separate reservoirs, i.e., a lossy medium and an amplifying medium (these reservoirs are respectively composed of pure particle absorbers and pure emitters): as a consequence, $S_l(\omega)$ and $S_p(\omega)$ are assumed to be perfectly independent and completely tunable physical quantities. A microscopic derivation of the Quantum Langevin Equation (2.1) illustrating all these features and based on a quantum optical model is presented in Sec. IV.

Finally we introduce the following quantity

$$\beta_{\text{eff}} \equiv \frac{1}{T_{\text{eff}}} \equiv \frac{S_l'(\omega_2) - S_p'(\omega_2)}{S_p(\omega_2)} = \frac{d}{d\omega} \log \left[\frac{S_l(\omega)}{S_p(\omega)} \right] \Big|_{\omega=\omega_2}. \quad (2.5)$$

As we will see in Sec. III, this model presents pseudo-thermalization properties at low energies for generic power spectra, and T_{eff} will play the role of an effective temperature. T_{eff} also scales like the linewidth of the power spectra Δ_{diss} and quantifies non-Markovianity, but unlike Δ_{diss} it is more sensitive to the local properties around ω_2 . In the Markovian limit, we have that $T_{\text{eff}}, \Delta_{\text{diss}} \rightarrow \infty$. On the contrary, for very steep power spectra (very coherent pump and/or loss processes), the dynamics is highly non-Markovian and we have that $T_{\text{eff}}, \Delta_{\text{diss}} \rightarrow 0$.

In analogy with what was already discussed in [33, 36], here the physical origins of the pseudo-thermalization can be understood intuitively at a qualitative level: at ω_2 losses and pump exactly compensate ($S_p(\omega_2) = S_l(\omega_2)$), so this frequency will play for this model the role of the condensate frequency (while ω_1 will be unstable), and frequencies close to this value will correspond to low-energy excitations on top of the condensate. However, close to ω_2 , the pump and loss power spectra verify the following condition (see Eq. (2.5)):

$$\frac{S_p(\omega_2 + \omega)}{S_l(\omega_2 + \omega)} \underset{\omega \rightarrow 0}{\simeq} (1 - \beta_{\text{eff}}\omega + \mathcal{O}(\omega/\Delta_{\text{diss}})^2) \sim e^{-\beta_{\text{eff}}\omega}, \quad (2.6)$$

so the Kennard-Stepanov relation [34, 35] is asymptotically verified at low frequencies. Thus, as we will demonstrate in Sec. III, steady-state low-energy properties are expected to be thermal.

Moreover, if we choose the pump and loss spectra to verify exactly the Kennard-Stepanov relation

$$\frac{S_p(\omega_2 + \omega)}{S_l(\omega_2 + \omega)} = e^{-\beta_{\text{eff}}\omega}, \quad (2.7)$$

then the system should thermalize at all energies. Note that this can be obtained without the various baths being at thermal equilibrium, as we can tune independently the pump and loss power spectra $S_{(l/p)}$ by changing the emitters and absorbers frequency distributions: namely, in Sec. IV we will discuss how the Kennard-Stepanov might be artificially arise in many physical contexts: first, we show this in Sec. IV B 2 with a specifically engineered quantum optical model by using a set of emitters with a non-trivial distribution of transition frequencies. Secondly, in Sec. IV C we show how the KS might be naturally reproduced exciton-polariton low-T experiments in some physical configurations where the scattering processes by longitudinal optical phonons are dominant.

All the results presented in the next sections regarding low-energy properties are general in the sense that they do not depend on the precise shape of the power spectra. Nonetheless, in order to substantiate the discussion, we performed numerical simulations for a specific choice of $S_{(l/p)}(\omega)$. For all the graphical representations we will thus consider the case of Markovian losses and a Lorentzian-shaped pump (see Fig. 1)

$$S_l^{\text{graph}}(\omega) \equiv \Gamma_l, \quad (2.8a)$$

$$S_p^{\text{graph}}(\omega) \equiv \Gamma_p \frac{(\Delta_{\text{diss}}/2)^2}{(\omega - \omega_p)^2 + (\Delta_{\text{diss}}/2)^2}. \quad (2.8b)$$

where the use of the notation Δ_{diss} is consistent with the previous definition. We also define the detuning $\delta \equiv \omega_0 - \omega_p$ between the photonic and the pump frequency. Accordingly, we need to have $\Gamma_l < \Gamma_p$ in order to obtain an amplified range of frequencies and generate a condensate, and $\omega_{1,2}$ are the two solutions of $\frac{(\Delta_{\text{diss}}/2)^2}{(\omega - \omega_p)^2 + (\Delta_{\text{diss}}/2)^2} = \frac{\Gamma_l}{\Gamma_p}$.

This choice of loss and pump power spectrum is naturally reproduced by our quantum optics proposal Sec. IV B 1.

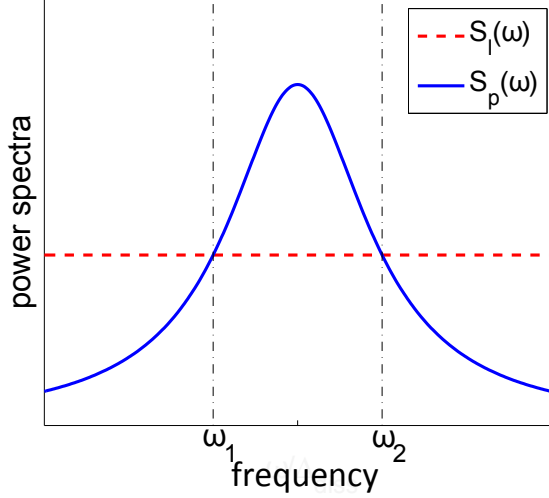


Figure 1: Power spectra for Markovian losses and Lorentzian shape pump in arbitrary units

Since it does not verify exactly the Kennard-Stepanov relation, we do not expect it will lead to complete thermalization; however, it is well suited to investigate the effect of low-energy pseudo-thermalization.

B. Non-interacting case

In this section we consider the case of a non-interacting Bose gas, i.e., we set the interaction strength g to 0. In this case, the Langevin equation Eq. (2.1) is linear and it can be solved exactly, for a given choice of $\Gamma(\omega)$. If a stationary state exists independent on the initial conditions (see discussion further below), one may evaluate the corresponding solution by introducing the Fourier transforms

$$\hat{\psi}_{\mathbf{k}}(\omega) = \int_{\mathbf{r},t} \hat{\psi}(\mathbf{r},t) e^{i(\mathbf{k}\cdot\mathbf{r}-\omega t)}, \quad (2.9a)$$

$$\hat{\psi}_{\mathbf{k}}^{\dagger}(\omega) = \int_{\mathbf{r},t} \hat{\psi}^{\dagger}(\mathbf{r},t) e^{-i(\mathbf{k}\cdot\mathbf{r}-\omega t)} = [\hat{\psi}_{\mathbf{k}}(\omega)]^{\dagger}, \quad (2.9b)$$

$$\hat{\xi}_{\mathbf{k}}(\omega) = \int_{\mathbf{r},t} \hat{\xi}(\mathbf{r},t) e^{i(\mathbf{k}\cdot\mathbf{r}-\omega t)}, \quad (2.9c)$$

$$\hat{\xi}_{\mathbf{k}}^{\dagger}(\omega) = \int_{\mathbf{r},t} \hat{\xi}^{\dagger}(\mathbf{r},t) e^{-i(\mathbf{k}\cdot\mathbf{r}-\omega t)} = [\hat{\xi}_{\mathbf{k}}(\omega)]^{\dagger}, \quad (2.9d)$$

and by replacing them into Eq. (2.1): one thus finds that the value of $\hat{\psi}_{\mathbf{k}}(\omega)$ is given by

$$\hat{\psi}_{\mathbf{k}}(\omega) = \frac{i\hat{\xi}_{\mathbf{k}}(\omega)}{\omega - \omega_0 - \epsilon_{\mathbf{k}} - i\Gamma(\omega)}, \quad (2.10)$$

with $\epsilon_{\mathbf{k}} = k^2/2m$. Note that, as a consequence of the absence of the non-linearity, all the modes \mathbf{k} are decoupled. When $\hat{\psi}_{\mathbf{k}}(\omega)$ is transformed back in real time, it results in a linear combination of several modes $\omega_{\mathbf{k},n}$, corresponding to the

poles of the denominator in Eq. (2.10), weighted with different amplitudes. For each value of \mathbf{k} , several solutions $\omega_{\mathbf{k},n}$ (labelled by the index n) may exist: this give rise to a branched spectrum of eigenfrequencies. The number of these branches depends on the peculiar choice of $\Gamma(\omega)$: these additional dispersions are related to the degrees of freedom which were integrated out from the dynamical description of the bosonic fields $\hat{\psi}$ and are accounted for by $\Gamma(\omega)$.

The imaginary part $\text{Im}[\omega_{\mathbf{k},n}]$ corresponds to the inverse life-time of the given mode: in order to have a dynamically stable mode, the condition $\text{Im}[\omega_{\mathbf{k},n}] < 0$ must be satisfied; this also implies that a dynamically stable stationary solution independent of the initial state exists, as any information on the initial state will vanish exponentially fast in time. On the contrary, if $\text{Im}[\omega_{\mathbf{k},n}] \geq 0$ for some values of \mathbf{k} and n , the corresponding mode grows indefinitely in time, or it remains constant: in both cases, one cannot neglect the information about the initial state, thus invalidating the assumption that a stationary value independent on the initial state exist. For $\text{Im}[\omega_{\mathbf{k},n}] > 0$, the field $\hat{\psi}$ diverges exponentially in time, and thus the solution is physically meaningless: nonetheless, this feature may signal a dynamical instability of the non-interacting approximation of Eq. (2.1), and, as a result, the inclusion of non-linearity may be crucial.

For the specific choice of the power spectra, discussed in the previous Section, which admits an amplifying region $[\omega_1, \omega_2]$, one expects some eigenmodes to present dynamical instabilities. Qualitatively, if $\omega_0 + \epsilon_{\mathbf{k}}$ falls into the amplifying region (which can be shifted with respect to $[\omega_1, \omega_2]$, due to the presence of the imaginary part $\text{Im}[\Gamma(\omega)]$ which induces a Lamb shift of the bare frequency), a dynamical instability is expected: while in a standard laser the instability would be controlled and ultimately stopped due to the presence of a saturated gain medium [40, 41], here those nonlinear terms were not included in our Langevin description. We will see below that the inclusion of a non-vanishing interaction strength $g \neq 0$ provides a non-standard saturation mechanism which prevents the unconstrained growth of dynamically unstable modes.

C. Interacting case: mean-field solution

We consider now the interacting solution of Eq. (2.1) for the interacting case $g \neq 0$. As a first level of approximation, we consider the classical limit of Eq. (2.1), which, in absence of a reservoir, corresponds to the well-known Gross-Pitaevskii description of a condensate [42]. This can be accomplished by replacing the quantum field $\hat{\psi}$ with a classical complex field ψ and by neglecting the quantum noise $\hat{\xi}$. The classical field ψ can be thus interpreted as the wave function of a condensate.

The validity of this approximation relies on the fact that the non-condensed fraction is assumed to be very small: this would have to be checked a posteriori by studying the effect of the fluctuations on the stability of the condensate solution (see Sec. II D). While in lower dimensional geometries, fluctuations are expected to be dominant [29, 30, 43] and thus preclude any such description, we expect that for high enough

spatial dimension d condensation is possible [26, 27]. Thus, a weak interaction coupling g (inducing a weak quantum depletion), and a certain selectivity in frequency of the dissipation (limiting the generation of excitations of high energy) should be suitable conditions for the emergence of coherence in the system. The classical field $\psi(\mathbf{r}, t)$ thus obeys the following equation:

$$\frac{\partial \psi(\mathbf{r}, t)}{\partial t} = -i \left[\omega_0 - \frac{\nabla^2}{2m} + g|\psi(\mathbf{r}, t)|^2 \right] \psi(\mathbf{r}, t) + \int_{\tau} \Gamma(\tau) \psi(\mathbf{r}, t - \tau), \quad (2.11)$$

which has the form of a driven-dissipative Gross-Pitaevskii equation with a memory kernel. We focus on spatially homogeneous solutions of the form

$$\psi(t) = \psi_0 e^{-i\omega_{\text{BEC}} t}, \quad (2.12)$$

which describe a condensate with infinite lifetime, frequency ω_{BEC} and density $n_0 = |\psi_0|^2$.

The non-condensed case $\psi_0 = 0$ is always a solution of Eq. (2.11), whose stability may be studied by linearizing Eq. (2.11) around it: this yields the linear equation studied in Sec. II B. As a result, the non-condensed solution is stable when the spectrum of the excitations lies outside the amplifying region, i.e., $\omega_0 + \epsilon_{\mathbf{k}} \geq \omega_2$. We will now show that non-trivial, condensed ($\psi_0 \neq 0$) solutions exist when the bare frequency lies below the upper-boundary of the amplifying region, i.e., $\omega_0 \leq \omega_2$. In this case, the interaction generates a blue-shift $\sim g n_0$ of the bosonic bare frequency ω_0 , thus providing a natural saturation mechanism as the condensate frequency is spontaneously set at one of the boundaries of the amplifying region. In fact, by inserting Eq. (2.12) into Eq. (2.11), one finds

$$\omega_{\text{BEC}} = \omega_0 + g|\psi_0|^2 + i\Gamma(\omega_{\text{BEC}}) \quad (2.13)$$

from which, by taking the real and the imaginary part and by using Eq. (2.4), one finds the two following equations for ω_{BEC} and $|\psi_0|^2$:

$$\mathcal{S}_p(\omega_{\text{BEC}}) = \mathcal{S}_l(\omega_{\text{BEC}}) \quad (2.14a)$$

$$\omega_{\text{BEC}} = \omega_0 + \mu + \delta_L(\omega_{\text{BEC}}), \quad (2.14b)$$

where

$$\mu \equiv g|\psi_0|^2 \quad (2.15)$$

is the mean-field self-interaction energy and

$$\delta_L(\omega) = \text{PV} \int_{\omega'} \frac{1}{\omega - \omega'} [\mathcal{S}_l(\omega') - \mathcal{S}_p(\omega')] \quad (2.16)$$

corresponds to a Lamb shift of the condensate frequency due to the contact with the bath. From Eq. (2.14a), we deduce that the only solutions for the condensate frequency are: $\omega_{\text{BEC}} = \omega_{1,2}$. However, the solution ω_1 will be unstable, since the low energy excitations of the condensate will fall in the amplified region $[\omega_1, \omega_2]$ and undergo dynamical instability,

thus we will not take into account this solution and consider in all the next sections the case $\omega_{\text{BEC}} = \omega_2$.

We finally remark that, unlike usual VCSEL [44] where stability is induced by a saturation effect of the pump (photonic emitters are 'two-level like' nonlinear systems which need some time to be repumped in the excited state), here stability is expected to be a consequence of the interplay between the frequency dependence of pumping and the progressive blue-shift $g|\psi_0|^2$ induced by interactions during the condensate growth, this until the condensate frequency reaches ω_{BEC} where pump and losses perfectly compensate.

D. Interacting case: Bogoliubov analysis of fluctuations

In order to study the stability of the condensate and to characterize the properties of its excitations, we express the bosonic field as

$$\hat{\psi}(\mathbf{r}, t) = [\psi_0 + \hat{\Lambda}(\mathbf{r}, t)] e^{-i\omega_{\text{BEC}} t}, \quad (2.17)$$

where $\hat{\Lambda}(\mathbf{r}, t)$ is an operator describing the fluctuations above the condensate. Inserting this decomposition and the mean-field solution obtained from Eq. (2.14) into Eq. (2.1), and retaining terms up to the first order in the fields $\hat{\Lambda}(\mathbf{r})$, $\hat{\Lambda}^\dagger(\mathbf{r})$, one obtains

$$\frac{\partial \hat{\Lambda}(\mathbf{r}, t)}{\partial t} = -i [\hat{\Lambda}(\mathbf{r}, t), H_{\text{bog}}(t)] + \int_{\tau} \tilde{\Gamma}(\tau) \hat{\Lambda}(\mathbf{r}, t - \tau) + \tilde{\xi}(\mathbf{r}, t) \quad (2.18)$$

where

$$H_{\text{bog}} = \int d^d r \left\{ \hat{\Lambda}^\dagger(\mathbf{r}) \frac{-\nabla^2}{2m} \hat{\Lambda}(\mathbf{r}) + \frac{\mu}{2} [2\hat{\Lambda}^\dagger(\mathbf{r}) \hat{\Lambda}(\mathbf{r}) + \hat{\Lambda}(\mathbf{r}) \hat{\Lambda}(\mathbf{r}) + \hat{\Lambda}^\dagger(\mathbf{r}) \hat{\Lambda}^\dagger(\mathbf{r})] \right\} \quad (2.19)$$

is the Bogoliubov Hamiltonian, $\tilde{\Gamma}$ is defined as

$$\tilde{\Gamma}(t) = e^{i\omega_{\text{BEC}} t} \Gamma(t) - \delta(t) \Gamma(\omega_{\text{BEC}}), \quad (2.20)$$

and $\tilde{\xi}(\mathbf{r}, t) = e^{i\omega_{\text{BEC}} t} \xi(\mathbf{r}, t)$. After calculation of the commutator, the equation Eq. (2.18) can be rewritten as

$$\frac{\partial \hat{\Lambda}(\mathbf{r}, t)}{\partial t} = -i \left\{ \frac{-\nabla^2}{2m} \hat{\Lambda}(\mathbf{r}, t) + \mu [\hat{\Lambda}(\mathbf{r}, t) + \hat{\Lambda}^\dagger(\mathbf{r}, t)] \right\} + \int_{\tau} \tilde{\Gamma}(\tau) \hat{\Lambda}(\mathbf{r}, t - \tau) + \tilde{\xi}(\mathbf{r}, t). \quad (2.21)$$

The linear system 2.21 can be regarded as the driven-dissipative non-markovian counterpart of the Bogoliubov-de Gennes equations. Similarly to the equilibrium case, the field $\hat{\Lambda}(\mathbf{r}, t)$ and its hermitian conjugate $\hat{\Lambda}^\dagger(\mathbf{r}, t)$ are coupled by the interaction energy μ : this coupling is mediated by processes in which non-condensed particles are scattered into the condensate, and vice-versa. It is convenient to rewrite Eq. (2.18) in momentum and frequency space: in order to do this, we define the Fourier transform of the fields and noise operators as

in Eq. (2.9). The correlations of the quantum noise operators in the momentum and frequency space are given by:

$$\langle \tilde{\xi}_{\mathbf{k}}(\omega) \tilde{\xi}_{\mathbf{k}'}^\dagger(\omega') \rangle = \delta_{\mathbf{k}-\mathbf{k}'} \delta_{\omega-\omega'} \mathcal{S}_I(\omega_{\text{BEC}} + \omega), \quad (2.22a)$$

$$\langle \tilde{\xi}_{\mathbf{k}}^\dagger(\omega) \tilde{\xi}_{\mathbf{k}'}(\omega') \rangle = \delta_{\mathbf{k}-\mathbf{k}'} \delta_{\omega-\omega'} \mathcal{S}_P(\omega_{\text{BEC}} + \omega). \quad (2.22b)$$

with $\delta_{\mathbf{k}} \equiv (2\pi)^d \delta^{(d)}(\mathbf{k})$, $\delta_\omega \equiv 2\pi\delta(\omega)$. After taking the Fourier transform of Eq. (2.18), we obtain the following set of coupled equations :

$$\omega \begin{pmatrix} \hat{\Lambda}_{\mathbf{k}}(\omega) \\ \hat{\Lambda}_{-\mathbf{k}}^\dagger(-\omega) \end{pmatrix} = \mathcal{L}_{\mathbf{k}}(\omega) \begin{pmatrix} \hat{\Lambda}_{\mathbf{k}}(\omega) \\ \hat{\Lambda}_{-\mathbf{k}}^\dagger(-\omega) \end{pmatrix} + i \begin{pmatrix} \tilde{\xi}_{\mathbf{k}}(\omega) \\ \tilde{\xi}_{-\mathbf{k}}^\dagger(-\omega) \end{pmatrix}, \quad (2.23)$$

where the matrix $\mathcal{L}_{\mathbf{k}}(\omega)$ is given by

$$\mathcal{L}_{\mathbf{k}}(\omega) = \begin{pmatrix} \epsilon_k + \mu + i\tilde{\Gamma}(\omega) & \mu \\ -\mu & -\epsilon_k - \mu + i\tilde{\Gamma}^*(-\omega) \end{pmatrix}, \quad (2.24)$$

where $\tilde{\Gamma}(\omega)$ is the Fourier transform of $\tilde{\Gamma}(t)$ defined in Eq. (2.20), and it reads:

$$\tilde{\Gamma}(\omega) = \Gamma(\omega + \omega_{\text{BEC}}) - \Gamma(\omega_{\text{BEC}}), \quad (2.25)$$

and we used the notation $\tilde{\Gamma}^*(\omega) \equiv [\tilde{\Gamma}(\omega)]^*$. The complex function $\tilde{\Gamma}(\omega)$ represents the frequency-dependent decay rate (real part) and lamb shift (imaginary part) of the fluctuations. $\tilde{\Gamma}(\omega)$ vanishes for $\omega \rightarrow 0$, consistently with the fact that the condensate has an infinite lifetime (see Eq. (2.13)).

For later convenience, we define the correlation matrix $\mathcal{C}_{\mathbf{k}}(\omega)$

$$\delta_{\mathbf{k}-\mathbf{k}'} \delta_{\omega-\omega'} \mathcal{C}_{\mathbf{k}}(\omega) = \begin{pmatrix} \langle \hat{\Lambda}_{\mathbf{k}}(\omega) \hat{\Lambda}_{\mathbf{k}'}^\dagger(\omega') \rangle & \langle \hat{\Lambda}_{\mathbf{k}}(\omega) \hat{\Lambda}_{-\mathbf{k}'}^\dagger(-\omega') \rangle \\ \langle \hat{\Lambda}_{-\mathbf{k}}^\dagger(-\omega) \hat{\Lambda}_{\mathbf{k}'}^\dagger(\omega') \rangle & \langle \hat{\Lambda}_{-\mathbf{k}}^\dagger(-\omega) \hat{\Lambda}_{-\mathbf{k}'}^\dagger(-\omega') \rangle \end{pmatrix}, \quad (2.26)$$

which can be calculated by inverting Eq. (2.23), multiplying the solution by its hermitian conjugate and averaging over the noise correlation using Eq. (2.22) (see App. VII A for the details of the calculations).

E. Dynamical stability of excitations

In order to study the dynamical stability of the mean-field solution, it is necessary to check that the elementary excitations do not grow exponentially and have a finite lifetime. To this end, we derive from Eq. (2.23) the excitations spectrum by calculating frequencies ω_k^i (with i some integer number used to label the excitation) which cancel out the determinant of the matrix $\omega - \mathcal{L}_{\mathbf{k}}(\omega)$ with $\mathcal{L}_{\mathbf{k}}(\omega)$ defined in Eq. (2.24). This leads us to the following condition on the frequency:

$$\left[\omega - \epsilon_k - \mu - i\tilde{\Gamma}(\omega) \right] \left[\omega + \epsilon_k + \mu - i\tilde{\Gamma}^*(-\omega) \right] + \mu^2 = 0. \quad (2.27)$$

Solutions with negative imaginary parts correspond to decaying excitations, while in presence of any instability, some solutions present a positive imaginary part. Since we are considering generic non-Markovian systems, $\tilde{\Gamma}(\omega)$ can be any

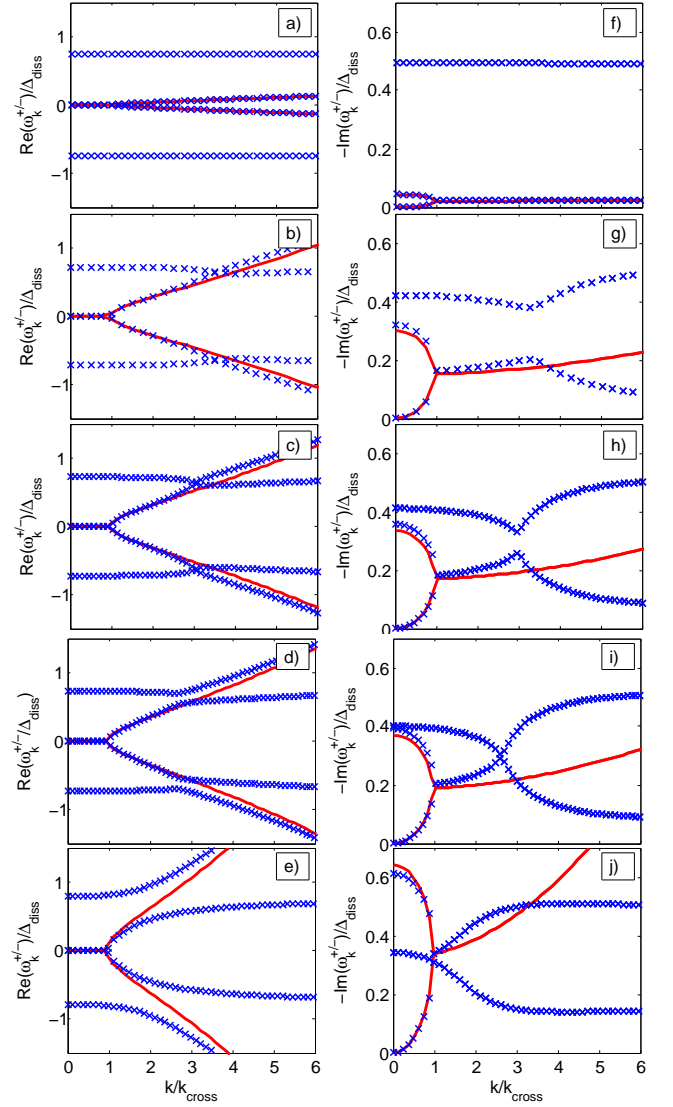


Figure 2: Excitation spectrum of the condensate in the case a Lorentzian pump spectrum and Markovian losses (model defined in Sec. II A). Left (resp. right) panel: real (resp. imaginary) part of the frequency in units of Δ_{diss} in function of the momentum k in units of k_{cross} defined as $|z_R|E_{k_{\text{cross}}} = z_I\mu$. In blue crosses we plot exact numerical solutions of the full non-Markovian theory (Eq. 2.23), and in red solid lines the solutions given by the corresponding Markovian effective theory at low energies (Eq. 2.31). Going from upper to lower panels, we investigate the transition between weak-dissipation to strong-dissipation. Parameters: $m = 1$, $\delta/\Delta_{\text{diss}} = 0$, $\Gamma_I/\Gamma_P = 0.3$. From up to down, $\Gamma_p^0/\Delta_{\text{diss}} = 0.1, 0.55, 0.6, 0.65, 1$.

function verifying the Kramers-Kronig relations reported in Eq. (2.4), thus in general Eq. (2.27) may have a large number of solutions, and it may be not possible to solve it analytically.

In the case of Markovian losses and a Lorentzian spectrum Eq. (2.8), Eq. (2.27) becomes an algebraic equation which admits four different solutions, thus giving rise to four different branches by varying the momentum k which we computed numerically. In Fig. 2, these solutions are plotted successively for increased values of $\Gamma_{(1/p)}$, going at fixed ratio $\Gamma_I/\Gamma_P = 0.3$

from a weakly-dissipative regime (upper panels) in which the spectral power $\Gamma_{(1/p)}$ are weak with respect to the linewidth Δ_{diss} , to a strong-dissipative regime (lower panels) in which they become comparable or higher. All other parameters (interaction g , mass m , detuning δ , linewidth Δ_{diss}) are left unchanged.

As a first observation, all imaginary parts of the frequencies are negative, so there is no instability (we checked this for other choice of parameters). Secondly, in the weak dissipative regime (panels a) and f)) the mode structure is typical of photonic driven-dissipative condensates [1, 21, 45, 46] and presents a sharp transition from purely damped modes to propagating ones. Also we observe two other branches of imaginary part Δ_{diss} and real parts $\pm(\omega_{\text{BEC}} - \omega_p)$: these additional frequencies account for the oscillation of bath degrees of freedom, which are hidden in the non-Markovianity of the Langevin equation and are nearly unaffected by the system dynamics due to the weak coupling (In a photonic language for the Lorentzian pump spectrum, the reservoir degrees of freedom responsible for the photonic pumping may be seen as two-level emitters of transition frequency ω_p).

However, for stronger dissipation (other panels), the system and reservoir degrees of freedom are coupled and can not be treated separately, which can be seen in a clearest way by a deformation of the various branches near the crossing point. Remarkably, a sharp transition from weak to strong coupling occurs between the panels c),h) and the panels d),i), inducing a change in excitation spectrum structure, as one moves from a situation of branch crossing to an avoided crossing: in this regime, the collective modes associated with the excitation spectrum couples the bosonic and the bath degrees of freedom, giving birth to a mixed quasi-excitation. In a photonic language, this suggests that some elementary excitations are of a polaritonic nature.

F. Effective low-frequency Markovian dynamics

An effective time-local equation describing the dynamics for frequencies small enough with respect to Δ_{diss} : indeed, for $\omega \ll \Delta_{\text{diss}}$, the function $\tilde{\Gamma}(\omega)$ defined in Eq. (2.23) can be linearized and approximated as $\tilde{\Gamma}(\omega) \approx \omega \tilde{\Gamma}'(0) = \omega \Gamma'(\omega_{\text{BEC}})$. As a result, the low-frequency limit of the Langevin equation Eq. (2.23) becomes:

$$\omega \hat{\Lambda}_{\mathbf{k}}(\omega) = z \left\{ \epsilon_k \hat{\Lambda}_{\mathbf{k}}(\omega) + \mu \left[\hat{\Lambda}_{\mathbf{k}}(\omega) + \hat{\Lambda}_{-\mathbf{k}}^\dagger(-\omega) \right] + i \bar{\xi}_{\mathbf{k}}(\omega) \right\}, \quad (2.28)$$

with the coefficient z defined as

$$z = \lim_{\omega \rightarrow 0} \left[\frac{\omega}{\omega - i \tilde{\Gamma}(\omega)} \right] = [1 - i \Gamma'(\omega_{\text{BEC}})]^{-1}, \quad (2.29)$$

and the new noise operators $\bar{\xi}_{\mathbf{k}}(\omega)$ and $\bar{\xi}_{\mathbf{k}}^\dagger(\omega)$ are characterized by the correlations

$$\langle \bar{\xi}_{\mathbf{k}}(\omega) \bar{\xi}_{\mathbf{k}'}^\dagger(\omega') \rangle = \delta_{\mathbf{k}-\mathbf{k}'} \delta_{\omega-\omega'} S_l(\omega_{\text{BEC}}), \quad (2.30a)$$

$$\langle \bar{\xi}_{\mathbf{k}}^\dagger(\omega) \bar{\xi}_{\mathbf{k}'}(\omega') \rangle = \delta_{\mathbf{k}-\mathbf{k}'} \delta_{\omega-\omega'} S_p(\omega_{\text{BEC}}). \quad (2.30b)$$

Notice that the noise operators $\bar{\xi}_{\mathbf{k}}(\omega)$ and $\bar{\xi}_{\mathbf{k}}^\dagger(\omega)$ correspond to an effective classical noise, since their correlations do not depend on the order of the operators, as a consequence of Eq. (2.14a).

With respect, to a purely hamiltonian dynamics, all couplings in the commutator have been multiplied by the complex number z . The eigenmodes of Eq. (2.28) are given by

$$\omega_k^\pm = -iz_I(\epsilon_k + \mu) \pm \sqrt{z_R^2 E_k^2 - z_I^2 \mu^2}, \quad (2.31)$$

where $z = z_R - iz_I$, z_R and z_I are both real numbers, and $E_k = \sqrt{\epsilon_k(\epsilon_k + 2\mu)}$ is the equilibrium Bogoliubov energy for the Hamiltonian Eq. (2.19). We can already verify the dynamical instability of the mean-field solution for the choice of BEC frequency $\omega_{\text{BEC}} = \omega_1$, as this leads to a negative z_I (due to a change of sign in the derivative of the real part of $\Gamma(\omega)$ involved in Eq. (2.29)) and thus to a positive imaginary part in the low-momentum excitation spectrum in Eq. (2.31). This justifies definitively the choice $\omega_{\text{BEC}} = \omega_2$ (whose dynamical stability was already checked in II E).

The frequencies ω_k^\pm , shown in Fig. 2 in red solid lines, closely resemble the spectrum of a polaritonic driven-dissipative condensate [1, 21, 45, 46]: they are imaginary for small momenta, which signals the purely diffusive nature of low-energy excitations, while they acquire a finite real part at higher momenta. In particular, for $k \rightarrow 0$ the branch ω_k^+ vanishes and therefore it can be identified with the (diffusive) Goldstone mode associated with the spontaneous breaking of the $U(1)$ symmetry. As was already discussed in the previous subsection, higher powers of ω present in Eq. (2.23) related to the non-Markovianity can generate additional modes not predicted by the effective low-energy theory Eq. (2.28), which can be observed in Fig. 2.

The validity of Eq. (2.28) for the study of the long-range physics has to be checked a posteriori, by requiring the absolute value $|\omega_k^\pm|$ to be small with respect to Δ_{diss} for small k , so that it can be computed by mean of the low-energy effective theory Eq. (2.28). On the one hand, this condition is naturally satisfied for the Goldstone branch ω_k^+ for low enough momenta. On the other hand, the gapped branch ω_k^- verifies $|\omega_{k=0}^-| = 2z_I\mu$, and therefore the gapped mode is correctly described by the Markovian low-frequency theory only if $2z_I\mu \ll \Delta_{\text{diss}}$. According to Eq. (2.29), z scales as $S_l(\omega_{\text{BEC}})/\Delta_{\text{diss}}$, so the gapped mode is correctly described by the Markovian low-frequency theory only if $S_l(\omega_{\text{BEC}})\mu \ll \Delta_{\text{diss}}^2$: this is the case for very small power spectra (weak dissipation) or very small interaction energy μ . The validity of this analysis is illustrated in Fig.2 where we can see that, within the range of applicability of our theory described below, the theoretical prediction Eq. (2.31) for the Goldstone mode and the gapped mode always fits with the exact numerical predictions.

III. PSEUDO-THERMALIZATION

In this section we give evidence for low-energy pseudo-thermalization for generic power spectra, both at static and

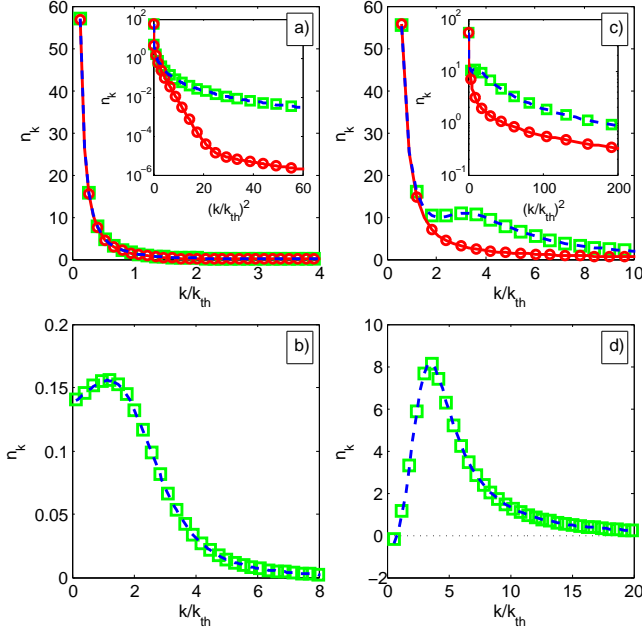


Figure 3: Static properties of the condensate at steady state in the weak dissipative regime (i.e., with the power spectra much smaller than Δ_{diss}) in the case of Lorentzian pump power spectrum and Markovian losses (model defined in Sec. II A). The left (resp. right) panels correspond to a detuning between the cavity and the atoms chosen to induce a weak (resp. strong) chemical potential μ with respect to the effective temperature T_{eff} . Upper panels: static correlations $n_{\mathbf{k}} = \langle \hat{\Lambda}_{\mathbf{k}}^\dagger \hat{\Lambda}_{\mathbf{k}} \rangle$ in function of the momentum \mathbf{k} in units of \mathbf{k}_{th} defined by $E(\mathbf{k}_{\text{th}}) = T_{\text{eff}}$, and in inset, their logarithm in function of the square momentum \mathbf{k}^2 in units of \mathbf{k}_{th}^2 . In green squares we plot the steady state properties given by numerical calculations of the linearized Langevin equation (Eq. (2.23)) in the weak dissipative regime, in red lines with circles the results given by the Grand-Canonical ensemble (Eq. (3.3)), and in dashed blue lines the analytical results given by the Fermi Golden's rule (Eq. (3.8)). Lower panels: the absolute error $n_{\mathbf{k}} - n_{\mathbf{k}}^{\text{th}}$ in green squares lines (resp. $n_{\mathbf{k}}^{\text{Fermi}} - n_{\mathbf{k}}^{\text{th}}$ in dashed blue lines) between the numerical solution of the Langevin equation (resp. the analytical solution given by the Fermi's golden rule) and the thermal case, in function of the momentum \mathbf{k} in units of \mathbf{k}_{th} . Parameters: for all panels, $m = 1$, $\Gamma_l/\Gamma_p^0 = 0.3$, $\Gamma_p/\Delta_{\text{diss}} = 10^{-2}$. Deduced quantity $T_{\text{eff}}/\Delta_{\text{diss}} = 0.55$. For the left (resp. right) panels: $\delta/\Delta_{\text{diss}} = 0.72$ (resp. -10). Deduced quantity $\mu/\Delta_{\text{diss}} = 4.6 \times 10^{-2}$ (resp. 10.8×10^0).

dynamical level, by showing that the low-energy static correlations map on equilibrium ones, and demonstrating the validity of the FDT in the low frequency regime. We also compute exactly the static correlations at all energies in the weakly dissipative regime. Finally, in the specific choice of reservoirs where the Kennard-Stepanov relation is exactly verified, we demonstrate the validity of FDT at all frequencies, and show that the steady-state in the weakly dissipative regime the steady-state is in a Gibbs ensemble.

A. Static correlations

A system presenting low-energy effective thermal properties should have steady state static properties similar to an equilibrium one, and look like a Gibbs ensemble at low-energies. In Sec. III A 1, we give the low-energy expression for static correlations, both in the weak and strong dissipative regimes, while in Sec. III A 2 we give an exact analytical expression at all energies, only valid in the weak-dissipative regime.

1. Low energies

In this section we focus on the low energy regime $E_{\mathbf{k}} \ll \Delta_{\text{diss}}$. By using the expression derived in Sec. VII A for the frequency-correlation matrix $C_{\mathbf{k}}(\omega)$ defined in Eq. (2.26) and by restricting ourselves to the low-frequency regime using the procedure described in Sec. II F, we compute by Fourier transform the steady state values of the momentum distribution $n_{\mathbf{k}} = \langle \hat{\Lambda}_{\mathbf{k}}^\dagger \hat{\Lambda}_{\mathbf{k}} \rangle$ and the anomalous average $\mathcal{A}_{\mathbf{k}} = \langle \hat{\Lambda}_{\mathbf{k}} \hat{\Lambda}_{-\mathbf{k}} \rangle$, at leading order for low energies (see App. VII B for the details of the calculation):

$$n_{\mathbf{k}} \simeq \frac{T_{\text{eff}} (\epsilon_{\mathbf{k}} + \mu)}{(E_{\mathbf{k}})^2}, \quad (3.1)$$

$$\mathcal{A}_{\mathbf{k}} \simeq -\frac{T_{\text{eff}} \mu}{(E_{\mathbf{k}})^2}, \quad (3.2)$$

where we remind that T_{eff} is defined in Eq. (2.5). These static correlations have to be compared to those obtained by doing a Bogoliubov calculation for a Bose gas at thermal equilibrium of temperature T_{eff} and chemical potential $\mu = g|\psi_0|^2$:

$$n_{\mathbf{k}}^{\text{th}} = \frac{1}{e^{\beta_{\text{eff}} E_{\mathbf{k}}} - 1} (|u_{\mathbf{k}}|^2 + |v_{\mathbf{k}}|^2) + |v_{\mathbf{k}}|^2 \quad (3.3)$$

$$\underset{(\beta_{\text{eff}} E_{\mathbf{k}}) \rightarrow 0}{\simeq} \frac{T_{\text{eff}} (\epsilon_{\mathbf{k}} + \mu)}{(E_{\mathbf{k}})^2},$$

$$\mathcal{A}_{\mathbf{k}}^{\text{th}} = 2 \left(\frac{1}{e^{\beta_{\text{eff}} E_{\mathbf{k}}} - 1} + \frac{1}{2} \right) u_{\mathbf{k}} v_{\mathbf{k}}^*, \quad (3.4)$$

$$\underset{(\beta_{\text{eff}} E_{\mathbf{k}}) \rightarrow 0}{\simeq} -\frac{T_{\text{eff}} \mu}{(E_{\mathbf{k}})^2},$$

where $u_{\mathbf{k}}$ and $v_{\mathbf{k}}$ relate (in the case of an isolated Bose Gas at equilibrium) the annihilation operator $\hat{\Lambda}_{\mathbf{k}}$ to the phonon annihilation (resp. creation) operator $\hat{b}_{\mathbf{k}}$ (resp. $\hat{b}_{\mathbf{k}}^\dagger$) through the Bogoliubov transformation:

$$\hat{\Lambda}_{\mathbf{k}} = u_{\mathbf{k}} \hat{b}_{\mathbf{k}} + v_{\mathbf{k}}^* \hat{b}_{\mathbf{k}}^\dagger, \quad (3.5)$$

$$u_{\mathbf{k}} = \frac{1}{2} \left[\sqrt{\frac{\epsilon_{\mathbf{k}}}{E_{\mathbf{k}}}} + \sqrt{\frac{E_{\mathbf{k}}}{\epsilon_{\mathbf{k}}}} \right], \quad (3.6)$$

$$v_{\mathbf{k}} = \frac{1}{2} \left[\sqrt{\frac{\epsilon_{\mathbf{k}}}{E_{\mathbf{k}}}} - \sqrt{\frac{E_{\mathbf{k}}}{\epsilon_{\mathbf{k}}}} \right]. \quad (3.7)$$

By comparing Eqs (3.1),(3.2) and Eqs. (3.3),(3.4), we note that the low-energy limit $\beta_{\text{eff}} E_{\mathbf{k}} \rightarrow 0$ of the driven-dissipative

quantum Langevin model accurately presents thermal-like infrared behaviour (the so-called Rayleigh-Jeans distribution). Higher energies correlations are not expected although to be thermal, and due to the algebraic behaviour of the Lorentzian pump power spectrum we do not expect in particular to see any exponential tails.

This analytical arguments can be verified in Fig.3 (resp. Fig. 4), where we plot the static correlations obtained by numerical resolution of the linearized Langevin equation for a Markovian loss spectrum and Lorentzian pump spectrum (Eq. (2.8)), in the weak-dissipative regime (resp. strong-dissipative regime), i.e. for $\Gamma_p^0, \Gamma_l \ll \Delta_{\text{diss}}$ (resp. Γ_p^0, Γ_l of the order of Δ_{diss}), and compare those correlations to thermal ones. We plotted the static correlations for two detunings δ of the bare frequency ω_0 with respect to the pump resonance ω_p , inducing different effective chemical potentials μ , which is a decreasing function of δ . Indeed, looking at Eq. (2.14b) and neglecting as a first step the Lamb shift, we see that increasing the frequency of the pump ω_p defined in Eq. (2.8), i.e., diminishing the detuning $\delta = \omega_0 - \omega_p$, has for effect to increase ω_{BEC} , and thus to increase also the chemical potential μ .

The case of a chemical potential weak (resp. strong) with respect to the effective temperature T_{eff} is plotted in the left (resp. right) panels. The upper panels correspond to the static correlations (with in insets their logarithm to check for any high-energy exponential tails), while in the lower panels we plot the absolute error $n_k - n_k^{\text{th}}$ between the solutions of the Langevin equations with respect to thermal predictions. Expectedly, static correlations given by the numerical simulation of the Langevin equation (green squares) coincide with the equilibrium results (red solid line with circles) at energies lower than the temperature (since T_{eff} scales as the spectra linewidth Δ_{diss} and is of the same order of magnitude), both in the weak and strong dissipative regimes. In particular, they diverge as $1/k^2$ at low momenta, and looking at the absolute errors we note that the corresponding corrections to thermal equilibrium remain finite at low energies and thus surprisingly do not present any subsingular divergencies $\propto 1/k$, so effective thermal equilibrium seems also to be true also at the next leading order at a static level for this particular system.

However, as we expected, the pseudo-thermalization does not extend for a generic choice of power spectra at higher energy scales (see the logarithmic plot) as the Kennard-Stepanov relation is not valid in this energy range: in particular, while one can see in the Grand Canonical distribution the presence of exponential tails of a Boltzmann type in the panel a) of Fig.3 (approximately for momenta verifying $k/k_{\text{th}}^2 \leq 20$, the kink at $k/k_{\text{th}}^2 = 20$ and the slower decay for higher momenta being related to the dominant vacuum fluctuations), such behaviour is not present in the driven-dissipative steady-state which rather features algebraic decay. This features is specifically related to the Lorentzian shape for the pump spectrum Eq. (2.8) chosen for numerical simulations. In the case of a big chemical potential $\mu > T_{\text{eff}}$ (see Fig.3 [panel c])), the thermal distribution does not present exponential tails neither because the vacuum fluctuations which decay algebraically are dominant with respect to thermal fluctuation in the energy

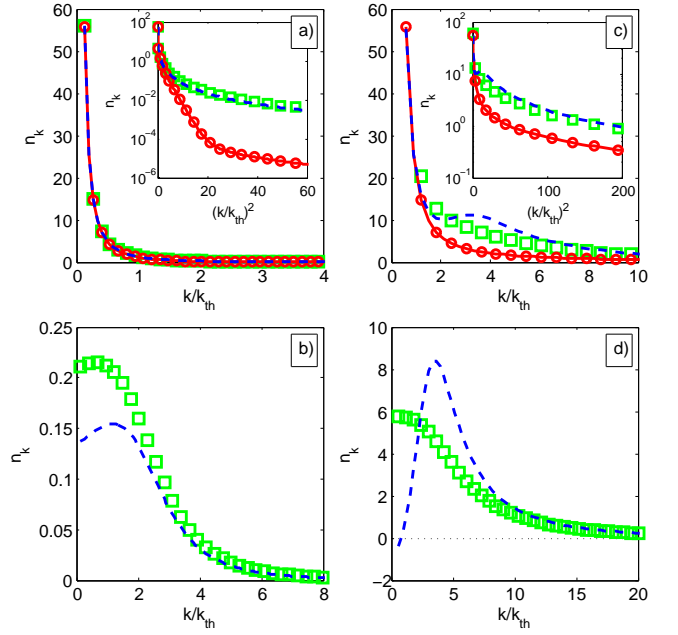


Figure 4: Static properties of the condensate at steady state in the strong dissipative regime (i.e. with the power spectra of the order of Δ_{diss}) in the case of Lorentzian pump spectrum and Markovian losses (model defined in Sec.II A). The left (resp. right) panels correspond to a detuning between the cavity and the atoms chosen to induce a weak (resp. strong) chemical potential μ with respect to the effective temperature T_{eff} . Upper panels: static correlations $n_k = \langle \Lambda_k^\dagger \Lambda_k \rangle$ in function of the momentum \mathbf{k} in units of \mathbf{k}_{th} defined by $E(\mathbf{k}_{\text{th}}) = T_{\text{eff}}$, and in inset, their logarithm in function of the square momentum \mathbf{k}^2 in units of \mathbf{k}_{th}^2 . In green squares we plot the steady state properties given by numerical calculations of the linearized Langevin equation (Eq. (2.23)) in the strong dissipative regime, in red line with circles the results given by the Grand-Canonical ensemble (Eq. (3.3)), and in dashed blue lines the analytical results given by the Fermi Golden's rule (Eq. (3.8)). Lower panels: the absolute error $n_k - n_k^{\text{th}}$ in green squares lines (resp. $n_k^{\text{Fermi}} - n_k^{\text{th}}$ in dashed blue lines) between the numerical solution of the Langevin equation (resp. the analytical solution given by the Fermi's golden rule) and the thermal case, in function of the momentum \mathbf{k} in units of \mathbf{k}_{th} . Parameters: for all panels, $m = 1$, $\Gamma_l/\Gamma_p = 0.3$, $\Gamma_p^0/\Delta_{\text{diss}} = 1$. Deduced quantity $T_{\text{eff}}/\Delta_{\text{diss}} = 0.55$. For the left (resp. right) panels: $\delta/\Delta_{\text{diss}} = 0.92$ (resp. -10). Deduced quantity $\mu/\Delta_{\text{diss}} = 7.3 \times 10^{-2}$ (resp. 11.0×10^0).

range $E_k \geq T_{\text{eff}}$.

2. Static correlations at all energies in the weakly dissipative regime

When the dissipation strength $\mathcal{S}_{(l/p)}(\omega)$ is much weaker than the linewidth of the power spectra Δ_{diss} , it is possible to provide exact analytical predictions for the static correlations

at all momenta:

$$n_{\mathbf{k}}^F = \frac{1}{K(E_k) - 1} (|u_{\mathbf{k}}|^2 + |v_{\mathbf{k}}|^2) + |v_{\mathbf{k}}|^2, \quad (3.8)$$

$$\mathcal{A}_{\mathbf{k}}^F = \left(\frac{1}{K(E_k) - 1} + \frac{1}{2} \right) u_{\mathbf{k}} v_{\mathbf{k}}^*. \quad (3.9)$$

Comparing these expressions to Eqs. (3.3),(3.4), we see that the vacuum properties are left unchanged with respect to equilibrium statistics, while the Boltzmann factor $e^{\beta E_k}$ of the Bose Einstein phononic distribution in the Grand canonical ensemble has been replaced by the non-equilibrium factor:

$$K(E_k) = \frac{S_l(\omega_{\text{BEC}} + E_k)|u_k|^2 + \mathcal{S}_p(\omega_{\text{BEC}} - E_k)|v_k|^2}{\mathcal{S}_p(\omega_{\text{BEC}} + E_k)|u_k|^2 + S_l(\omega_{\text{BEC}} - E_k)|v_k|^2}, \quad (3.10)$$

giving thus rise to the modified Bose Einstein phonon distribution $\frac{1}{K(E_k)-1}$. The factor $K(E_k)$ can be interpreted as the ratio between the annihilation and creation rates (both induced by pumping and losses dissipative processes) of a single phononic excitation at the Bogoliubov energy E_k , and is calculated using the secular approximation (valid in the weakly dissipative regime). The phonon distribution and average occupation number are a consequence of detailed balance between states with $N_{\mathbf{k}}$ and $N_{\mathbf{k}} - 1$ phonons of momentum \mathbf{k} . We note that if the pumping and loss rates verify the Kennard-Stepanov condition Eq. (2.7), one recovers the equilibrium Boltzmann factor $K(E_k) = e^{\beta E_k}$: as expected the system is fully thermal at all energies, and its density matrix at steady-state is a Grand-Canonical ensemble. In the general case by using Eq. (2.5) we note that $K(E_k) \underset{E_k \rightarrow 0}{\sim} 1 - \beta_{\text{eff}} E_k \sim e^{-\beta_{\text{eff}} E_k}$: this provides us another confirmation that low-energy static properties should be thermal.

Static correlations of Eqs. (3.8),(3.9) computed under the secular approximation are shown in dashed blue lines in the upper panels of Fig. 3 (resp. Fig. 4) and compared with the numerical results Langevin equation in the weak (resp. strong) dissipative regime. In the lower panels we plot the absolute error $n_k^{\text{Secular}} - n_k^{\text{th}}$ between the solution given by the secular approximation and the thermal distribution. We note absolutely no difference between the exact numerical solution and n_k^{Secular} . Expectedly, in the strong-dissipative regime they coincide only at low momenta ($E_k \ll T_{\text{eff}}$) (up to a finite error, which is small with respect to the divergency in $1/k^2$), and do not provide exact results at higher momenta.

We now justify the expression Eqs. (3.8),(3.9) for the static correlations in the weak dissipative regime $\mathcal{S}_p, S_l \ll \Delta_{\text{diss}}$ by applying the secular approximation: we consider dissipation as a "classical" stochastic process inducing transitions in the system S between the hamiltonian eigenstates populations, i.e., the diagonal coefficients of the bosonic density matrix $\rho_S = \text{Tr}_B(\rho)$ (which corresponds to the partial trace of the full density matrix ρ over the various baths) in the eigenbasis of the Bogoliubov hamiltonian H_{bog} (defined in Eq. (2.19)). These eigenstates are defined in the equilibrium phononic basis: $\otimes_{\mathbf{k}} |N_{\mathbf{k}}\rangle$, where \mathbf{k} is the momentum and $N_{\mathbf{k}}$ is the occupation number of the phonon of momentum \mathbf{k} . The

phonon annihilation and creation operators $\hat{b}_{\mathbf{k}}$ and $\hat{b}_{\mathbf{k}}^\dagger$ are related to the particle annihilation and creation operators $\hat{\Lambda}_{\mathbf{k}}$ and $\hat{\Lambda}_{\mathbf{k}}^\dagger$ by the Bogoliubov transformation Eq. (3.5).

Phonon annihilation rate: Let us calculate as a first step the phononic annihilation rate. Starting from a state with $N_{\mathbf{k}}$ phonons of momentum \mathbf{k} and Bogoliubov energy E_k , one can remove one phonon through two processes:

- First, one can remove a phonon by losing a particle of momentum \mathbf{k} . The total energy removed to the system is $\omega_{\text{BEC}} + E_k$. This leads to the partial rate:

$$\begin{aligned} \mathcal{T}^{(l)}(N_{\mathbf{k}} \rightarrow N_{\mathbf{k}} - 1) &= S_l(\omega_{\text{BEC}} + E_k) \left| \langle N_{\mathbf{k}} - 1 | \hat{\Lambda}_{\mathbf{k}} | N_{\mathbf{k}} \rangle \right|^2 \\ &= S_l(\omega_{\text{BEC}} + E_k) N_{\mathbf{k}} |u_{\mathbf{k}}|^2. \end{aligned} \quad (3.11)$$

Starting from a wave-function calculation, this expression could have been alternatively recovered by mean of the Fermi's Golden rule [47].

- However, due to the presence of counter-rotating terms in the Bogoliubov theory, it is also possible to remove a phonon by pumping a particle of momentum $-\mathbf{k}$. The total energy added to the system in that case is $\omega_{\text{BEC}} - E_k$, i.e, the mean-field energy of a single phonon, minus the energy of the phonon excitation. Thus the corresponding rate is:

$$\begin{aligned} \mathcal{T}^{(p)}(N_{\mathbf{k}} \rightarrow N_{\mathbf{k}} - 1) &= \mathcal{S}_p(\omega_{\text{BEC}} - E_k) \\ &\quad \times \left| \langle N_{\mathbf{k}} - 1 | \hat{\Lambda}_{\mathbf{k}}^\dagger | N_{\mathbf{k}} \rangle \right|^2 \\ &= \mathcal{S}_p(\omega_{\text{BEC}} - E_k) N_{\mathbf{k}} |v_{\mathbf{k}}|^2 \end{aligned} \quad (3.12)$$

The total phonon loss rate is thus:

$$\begin{aligned} \mathcal{T}^{(tot)}(N_{\mathbf{k}} \rightarrow N_{\mathbf{k}} - 1) &= S_l(\omega_{\text{BEC}} + E_k) N_{\mathbf{k}} |u_{\mathbf{k}}|^2 \\ &\quad + \mathcal{S}_p(\omega_{\text{BEC}} - E_k) N_{\mathbf{k}} |v_{\mathbf{k}}|^2. \end{aligned} \quad (3.13)$$

Phonon creation rate: One can calculate similarly the phonon total creation rate. Starting from a state with $N_{\mathbf{k}} - 1$ phonons of momentum \mathbf{k} and Bogoliubov energy E_k , one can add one phonon by pumping a new particle (the total energy added to the system is thus $\omega_{\text{BEC}} + E_k$) or by losing a particle (the total energy lost is $\omega_{\text{BEC}} - E_k$). After a calculation very similar to the previous paragraph, one obtains the following expression:

$$\begin{aligned} \mathcal{T}^{(tot)}(N_{\mathbf{k}} - 1 \rightarrow N_{\mathbf{k}}) &= \mathcal{S}_p(\omega_{\text{BEC}} + E_k) N_{\mathbf{k}} |u_{\mathbf{k}}|^2 \\ &\quad + S_l(\omega_{\text{BEC}} - E_k) N_{\mathbf{k}} |v_{\mathbf{k}}|^2. \end{aligned} \quad (3.14)$$

Phonon probability distribution: The ratio between the phonon annihilation and creation rates is given by

$$\begin{aligned} K(E_k) &= \frac{\mathcal{T}^{(tot)}(N_{\mathbf{k}} \rightarrow N_{\mathbf{k}} - 1)}{\mathcal{T}^{(tot)}(N_{\mathbf{k}} - 1 \rightarrow N_{\mathbf{k}})} \\ &= \frac{S_l(\omega_{\text{BEC}} + E_k)|u_k|^2 + \mathcal{S}_p(\omega_{\text{BEC}} - E_k)|v_k|^2}{\mathcal{S}_p(\omega_{\text{BEC}} + E_k)|u_k|^2 + S_l(\omega_{\text{BEC}} - E_k)|v_k|^2}. \end{aligned} \quad (3.15)$$

Because dissipation processes can remove or add only one phonon of momentum \mathbf{k} at a time and do not affect simultaneously the other momenta, one deduces that at steady state, the probabilities $\pi(\dots, N_{\mathbf{k}} - 1, \dots)$ and $\pi(\dots, N_{\mathbf{k}}, \dots)$ of having $N_{\mathbf{k}} - 1$ and $N_{\mathbf{k}}$ phonons of momentum \mathbf{k} (leaving the occupation numbers other momenta \mathbf{k}' unchanged) verify the following detailed balance relation :

$$\pi(N_{\mathbf{k}} - 1) = K(E_{\mathbf{k}})\pi(N_{\mathbf{k}}). \quad (3.16)$$

One deduces that the probability distribution is

$$\pi(N_{\mathbf{k}}) = \frac{1}{1 - K(E_{\mathbf{k}})^{-1}} K(E_{\mathbf{k}})^{-n}, \quad (3.17)$$

and that the average phonon occupation number is

$$n_{\mathbf{k}}^{(phonon)} = \frac{1}{K(E_{\mathbf{k}}) - 1}. \quad (3.18)$$

Doing a Bogoliubov transformation Eq. (3.5), one obtains the momentum static distribution and anomalous averages Eqs. (3.8),(3.9).

B. Effective temperature from FDT

A remarkable consequence of equilibrium which involves dynamical quantities is the so-called fluctuation-dissipation theorem [39], which provides a relationship between the linear response of a system to an external perturbation and the correlation of thermal fluctuations.

Let us define the symmetrized correlation (C) and response (R) functions for two arbitrary operators \hat{A} and \hat{B} as

$$iC(t - t') = \langle \{\hat{A}(t), \hat{B}(t')\} \rangle, \quad (3.19a)$$

$$iR(t - t') = \theta(t - t') \langle [\hat{A}(t), \hat{B}(t')] \rangle, \quad (3.19b)$$

where the time dependence of $\hat{A}(t)$ and $\hat{B}(t)$ is determined in the Heisenberg picture, while the average $\langle \dots \rangle$ is taken over an equilibrium state at temperature T . As a consequence of equilibrium, C and R depend only on the time difference $t - t'$ and therefore we can define their Fourier transforms $C(\omega)/R(\omega) = \int_t e^{i\omega t} C(t)/R(t)$. The explicit form of the FDT then reads:

$$C(\omega) = 2 \coth(\beta\omega/2) \text{Im}[R(\omega)], \quad (3.20)$$

with $\beta = T^{-1}$. An alternative, fully equivalent formulation of the FDT is the so-called Kubo-Martin-Schwinger (KMS) [48, 49] condition:

$$S_{AB}(-\omega) = e^{-\beta\omega} S_{BA}(\omega), \quad (3.21)$$

where $S_{AB}(t) = \langle \hat{A}(t)\hat{B} \rangle$ and $S_{BA}(t) = \langle \hat{B}(t)\hat{A} \rangle$.

The FDT and KMS condition have often been used as a tool to probe the actual thermalization in classical and quantum systems, and to characterize the eventual departure from equilibrium [32, 50, 51]. In particular, from Eqs. (3.20) and (3.21)

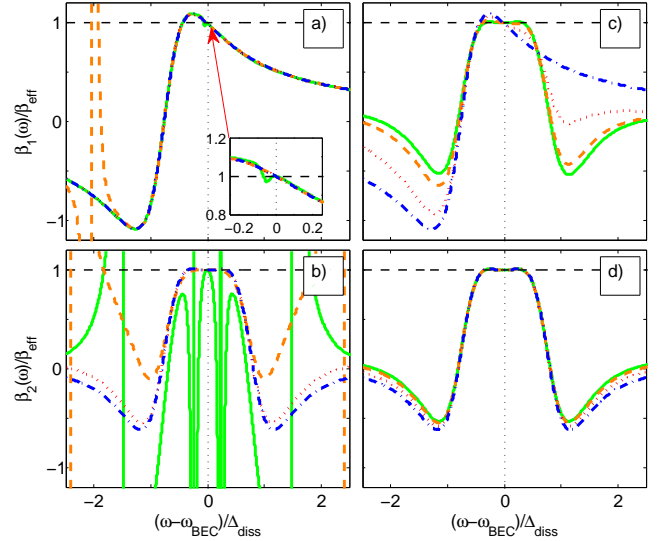


Figure 5: Test of the FDT/KMS relations for various sets of parameters. Upper (resp. lower) panels: plot of the frequency dependent effective temperature $\beta_{1,\text{eff}}(\mathbf{k}, \omega)$ (resp. $\beta_{2,\text{eff}}(\mathbf{k}, \omega)$) defined in Eq. (2.5) for a Lorentzian pump and Markovian losses, in function of the frequency $\omega - \omega_{\text{BEC}}$ in units of Δ_{diss} , and for various momenta \mathbf{k} . Panels a),b) (resp. c),d)) use the same parameters as in the panels a),b) (resp. c),d)) of Fig. 3. For each panel, the various curves corresponds to increasing momenta chosen in such a way that the corresponding Bogoliubov spectrum spans all energy below and above the resulting effective temperature $T_{\text{eff}} = 0.54\Delta_{\text{diss}}$: $k/k_{\text{th}} = 0.18$ for the green solid line, $k/k_{\text{th}} = 3.65$, for the orange dashed line, $k/k_{\text{th}} = 9.1$ for the red dotted line, $k/k_{\text{th}} = 54.7$ for the blue dash-dotted line

one can define an effective frequency-dependent temperature $T_{A,B,\text{eff}}(\omega)$ such that FDT or KMS condition are satisfied: if the system is really at equilibrium, then $T_{A,B,\text{eff}}(\omega)$ has a constant value T which corresponds to the thermodynamic temperature. On the other hand, if the system is out of equilibrium it will generically develop a non-trivial dependence on A , B and ω .

In the following, we discuss the effective temperatures obtained from the linearized equation Eq. (2.18): in this respect, we will consider the following ratios:

$$\frac{\langle \hat{\Lambda}_{\mathbf{k}}(\omega) \hat{\Lambda}_{\mathbf{k}}^\dagger \rangle}{\langle \hat{\Lambda}_{\mathbf{k}}^\dagger(\omega) \hat{\Lambda}_{\mathbf{k}} \rangle} = \frac{\mathcal{S}_l(\omega_{\text{BEC}} + \omega) + \mathcal{S}_p(\omega_{\text{BEC}} - \omega) A_k(\omega)}{\mathcal{S}_p(\omega_{\text{BEC}} + \omega) + \mathcal{S}_l(\omega_{\text{BEC}} - \omega) A_k(\omega)}, \quad (3.22)$$

$$\frac{\langle \hat{\Lambda}_{\mathbf{k}}(\omega) \hat{\Lambda}_{-\mathbf{k}} \rangle}{\langle \hat{\Lambda}_{\mathbf{k}}^\dagger(-\omega) \hat{\Lambda}_{-\mathbf{k}} \rangle} = \frac{\mathcal{S}_l(\omega_{\text{BEC}} + \omega) + \mathcal{S}_p(\omega_{\text{BEC}} - \omega) B_k(\omega)}{\mathcal{S}_p(\omega_{\text{BEC}} + \omega) + \mathcal{S}_l(\omega_{\text{BEC}} - \omega) B_k(\omega)}, \quad (3.23)$$

where the functions $A_k(\omega)$ and $B_k(\omega)$ are explicitly reported in App. VII A. At thermal equilibrium, the value of the ratios (3.22) and (3.23) is fixed by Eq. (3.21) while, in the present case, they have a nontrivial dependence on ω and k , since the system is out of equilibrium.

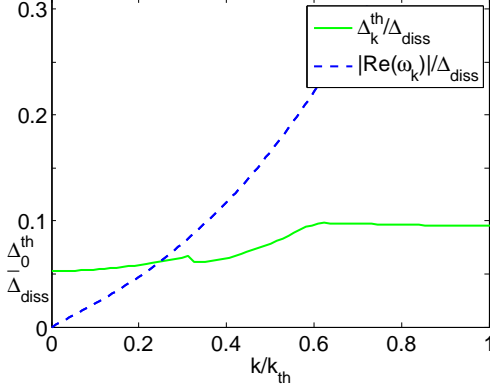


Figure 6: Test of the efficiency of thermalization in function of the momentum k in units of k_{th} . In green solid line, one shows Δ_k^{th} (in units of Δ_{diss}), defined as the maximum frequency such that both conditions $|\beta_1(\mathbf{k}, \omega) - \beta_{eff}|/\beta_{eff} \leq 0.05$ and $|\beta_2(\mathbf{k}, \omega) - \beta_{eff}|/\beta_{eff} \leq 0.05$ are verified for all ω contained in the interval $|\omega - \omega_{BEC}| \leq \Delta_k^{th}$. In dashed blue lines, one shows in absolute value the real part $|\text{Re}(\omega_k)|$ (in units of Δ_{diss}) of the dissipative Bogoliubov spectrum for the same parameters, computed by exact numerical calculation of the solutions of Eq. (2.27) (the other branches are not visible here since located at higher energies). Same parameters as in Fig. 5 a),b)

We then define the effective (inverse) temperatures

$$\beta_{1,eff}(\mathbf{k}, \omega) = \frac{d}{d\omega} \log \left[\frac{\langle \hat{\Lambda}_{\mathbf{k}}(\omega) \hat{\Lambda}_{\mathbf{k}}^\dagger \rangle}{\langle \hat{\Lambda}_{\mathbf{k}}^\dagger(\omega) \hat{\Lambda}_{\mathbf{k}} \rangle} \right], \quad (3.24)$$

$$\beta_{2,eff}(\mathbf{k}, \omega) = \frac{d}{d\omega} \log \left[\frac{\langle \hat{\Lambda}_{\mathbf{k}}(\omega) \hat{\Lambda}_{-\mathbf{k}} \rangle}{\langle \hat{\Lambda}_{\mathbf{k}}(-\omega) \hat{\Lambda}_{-\mathbf{k}} \rangle} \right], \quad (3.25)$$

which are generic functions of k and ω , and can be evaluated by using Eqs. (3.22) and (3.23). However, inserting the functional forms Eqs. (3.22), (3.23) into Eqs. (3.24), (3.25) we see that for $\omega \rightarrow 0$, both $\beta_{1,eff}(\mathbf{k}, \omega)$ and $\beta_{2,eff}(\mathbf{k}, \omega)$ tend toward the same k -independent value β_{eff} defined in Eq. (2.5), indicating that the KMS condition and the FDT are asymptotically verified at low frequencies.

Remarkably, if the system satisfies the Kennard-Stepanov relation

$$\mathcal{S}_p(\omega_{BEC} + \omega) = \mathcal{S}_l(\omega_{BEC} + \omega) e^{-\beta\omega}, \quad (3.26)$$

then $\beta_{1,eff}(\mathbf{k}, \omega) = \beta_{2,eff}(\mathbf{k}, \omega) = \beta$ for every value of ω and \mathbf{k} , i.e., the system is at full thermal equilibrium, even if the environment is highly non-thermal (see Secs. IV B 2, IV C for examples of physical systems made of non-thermal reservoirs verifying artificially the KS relation).

In Fig. 5, we plot the effective temperature $\beta_{1,eff}(\mathbf{k}, \omega)$ (resp. $\beta_{2,eff}(\mathbf{k}, \omega)$) in the left panel (resp. right panel) in function ω in units of Δ_{diss} , for various momenta \mathbf{k} . We notice first that in the region $\omega \ll \Delta_{diss}$, these effective temperatures converge to the same value β_{eff} confirming thus the low-frequency validity of FDT, and that the system is effectively thermalized in that frequency range. Away from that region

they have a non-trivial, frequency-momentum dependent behaviour, so the system is globally not at equilibrium.

Strikingly, it appears that FDT is completely verified below a certain energy cutoff Δ_0^{th} (for these precise simulations $\Delta_0^{th} \simeq 0.05 \times \Delta_{diss} \simeq 0.1 \times T_{eff}$) as shown in Fig. 6: for frequencies close enough to the condensate frequency $|\omega - \omega_{BEC}| \leq \Delta_0^{th}$, we observe that excitations at any momenta feature frequency-dependent effective temperatures $\beta_{1/2}(\omega)$ presenting less than 5% deviation from the limit value β_{eff} (this error can be arbitrarily reduced by getting closer to ω_{BEC}). In particular, the green solid line in Fig. 5 b) shows the worst case scenario, which occurs to $\beta_2(\omega)$ in the limit $k \rightarrow 0$ (we have checked for any momenta that the singularities[53] of $\beta_2(\omega)$ can not get any closer to ω_{BEC}). As a consequence, all the low-energy elementary excitations of the condensate, whose counterpart in the isolated equilibrium case possesses a Bogoliubov energy $E_k \leq \Delta_0^{th}$ will have their resonance located in the thermalized frequency window $[\omega_{BEC} - \Delta_0^{th}, \omega_{BEC} + \Delta_0^{th}]$ and will verify FDT at a very good level of approximation. Remarkably, for this simulation $\Delta_0^{th} \geq \mu \simeq 0.045 \times \Delta_{diss}$, meaning that not only the phononic region of the spectrum is efficiently thermalized, but also the transient phonon-particle regime and a part of the particle excitations.

IV. DERIVATION OF THE LANGEVIN EQUATION FROM A QUANTUM OPTICS MICROSCOPIC MODEL

In this section, we proceed to the derivation of the Langevin equation (2.1) in an array spatial geometry, starting from the microscopic quantum optics model introduced in [33]. Namely, we consider a photonic driven-dissipative Bose-Hubbard lattice made of L nonlinear cavities coupled by tunneling. Each cavity possesses a natural frequency ω_0 and is assumed to contain a $\chi^{(3)}$ Kerr nonlinear medium, which induces effective repulsive interactions between photons lying in the same cavity. Dissipative phenomena due finite mirror transparency and absorption by the cavity material are responsible for (possibly non-Markovian) loss processes.

We assume that a number N_{at} of two-level atoms are embedded in each cavity in order to inject new photons to compensate losses, and that the atomic transition $\omega_{at}^{(n)}$ frequencies possess some frequency distribution $\mathcal{D}(\omega)$. Each atom is strongly pumped at a rate Γ_p^{at} (in such a way that its spontaneous decay can be neglected), and is coupled to the cavity with a Rabi frequency Ω_R , which is assumed to be weak enough ($\Omega_R \ll \omega_{at}^{(n)}, \omega_0$) in order to stay far from the ultra-strong coupling regime.

The dissipative effects related to the atomic pumping and photonic losses processes can be described in terms of the coupling of the photon-atom system to various reservoirs, and the whole system dynamics can thus be described by an Hamiltonian involving the photonic and atomic degrees of freedom plus an external environment:

$$H = H_{ph} + H_{at} + H_{bath} + H_I \quad (4.1)$$

The Hamiltonian for the isolated photonic system has the usual Bose-Hubbard form :

$$H_{\text{ph}} = \sum_{i=1}^L \left[\omega_0 a_i^\dagger a_i + \frac{U}{2} a_i^\dagger a_i^\dagger a_i a_i \right] - \sum_{\langle i,j \rangle} \left[\hbar J a_i^\dagger a_j + h c \right] : \quad (4.2)$$

We assumed that the Kerr nonlinearity of the cavity medium induces an on-site interaction term U . The free evolution of the atoms is described by the following Hamiltonian

$$H_{\text{at}} = \sum_{i=1}^L \sum_{n=1}^{N_{\text{at}}} \omega_{\text{at}}^{(n)} \sigma_i^{(n)+} \sigma_i^{(n)-}. \quad (4.3)$$

The baths, modelled as a reservoir of harmonic oscillators, are represented by the following Hamiltonian:

$$H_{\text{bath}} = \sum_{i=1}^L \sum_m \left[\omega_m b_i^{(m)\dagger} b_i^{(m)} - \sum_{n=1}^{N_{\text{at}}} \tilde{\omega}_m c_i^{(n,m)\dagger} c_i^{(n,m)} \right]. \quad (4.4)$$

The indices i, n, m account respectively for the cavity modes, the atoms, and the bath excitations. The full interaction hamiltonian, between photons, atoms and bath excitations is given by :

$$H_{\text{I}} = \Omega_{\text{R}} \sum_{i,n} \left[a_i^\dagger \sigma_i^{-(n)} + h c \right] + \sum_{i,m} g_m \left[a_i^\dagger b_i^{(m)} + h c \right] + \sum_{i,n,m} \tilde{g}_m \left[\sigma_i^{+(n)} c_i^{\dagger(n,m)} + h c \right]. \quad (4.5)$$

Remarkably, unlike the photonic field $a_i^{(m)}$ which is coupled to the bath by mean of a creation operator $b_i^{(m)\dagger}$ in order to account for loss processes, the atomic raising operator $\sigma_i^{+(n)}$ is coupled in an anti-rotating way to a creation operator $c_i^{\dagger(n,m)}$ so to reproduce the effect of an irreversible atomic pumping leading to an inversion of population. This process is compatible with energy conservation as the harmonic oscillator $c_i^{(n,m)}$ possesses a negative frequency $-\tilde{\omega}_m$.

While such a reservoir might look a bit artificial at first glance, physically an irreversible pumping can be obtained by coherently coupling the atomic ground-state to an hidden third atomic level with a strong decay toward the first excited state, in analogy with the lasing operation [40]. For simplicity purpose, we also made the assumption that each atom is coupled to a different pumping bath, i.e, a different set of harmonic oscillators. While this can be obtained when atoms are spatially separated enough, extending this derivation to the case of a single bath for atomic pumping is straightforward and leads to similar physics. We assume both baths to be in the vacuum state at the initial time

$$\langle b_i^{(m)\dagger} b_i^{(m)} \rangle (0) = \langle c_i^{(n,m)\dagger} c_i^{(n,m)} \rangle (0) = 0 : \quad (4.6)$$

meaning that the bath $b_i^{(m)}$ (resp. $c_i^{(n,m)}$) can only induce photon losses (resp. atomic excitation). The various baths are

also assumed to have a broad spectral function

$$\sum_m |g_m|^2 e^{-i\omega_m \tau} = \int_{\omega} \mathcal{S}_1(\omega) e^{-i\omega \tau} \quad (4.7)$$

$$\sum_m |\tilde{g}_m|^2 e^{-i\tilde{\omega}_m \tau} = \Gamma_{\text{p}}^{\text{at}} \delta(\tau), \quad (4.8)$$

where $\mathcal{S}_1(\omega)$ is the loss power spectra of a single cavity, and the atomic pumping processes are described as Markovian.

We finally put ourselves in the regime where the atomic pumping rate $\Gamma_{\text{p}}^{\text{at}}$ is big enough with respect to the Rabi Coupling Ω_{R} , in such a way that during dynamics atoms spend most of their time in the excited state and very little in the ground-state (to do so and maintain at the same time the photonic total pumping rate fixed at the desired intensity, one can embed a large enough number of atoms within the whole system, while diminishing correspondingly their individual Rabi coupling Ω_{R} to the cavity mode). In consequence, a single atom will have a very weak probability to be in the ground-state, the effect of atomic saturation of the photonic pump will be very reduced and atoms will behave as linear degrees of freedom. We can thus replace the spin matrix of each atomic two-level system by an ‘inverse’ harmonic oscillator whose vacuum state (resp. whose state with a single excitation) corresponds to the atomic excited state (resp. to the atomic ground-state): $a_{\text{at},i}^{(n)} \equiv \sigma_i^{(n)+}$. States of the harmonic oscillator with more than one excitation will be so rarely occupied that they will not contribute to the photonic dynamics.

We obtain thus the modified (although physically equivalent for our choice of parameters) atomic and interaction Hamiltonians:

$$H_{\text{at}} = \sum_{i=1}^{N_{\text{cav}}} \sum_{k=1}^{N_{\text{at}}} (-\omega_{\text{at}}^{(n)}) a_{\text{at},i}^{(n),\dagger} a_{\text{at},i}^{(n)} + E_0 \quad (4.9)$$

where E_0 is a constant, and

$$H_{\text{I}} = \Omega_{\text{R}} \sum_{i,n} \left[a_i^\dagger a_{\text{at},i}^{(n),\dagger} + h c \right] + \sum_{i,m} g_m \left[a_i^\dagger b_i^{(m)\dagger} + h c \right] + \sum_{i,n,m} \tilde{g}_m \left[c_i^{(n,m)\dagger} a_{\text{at},i}^{(n)} + h c \right]. \quad (4.10)$$

In our description the harmonic oscillator $a_{\text{at},i}^{(n)}$ and the excitations bath $c_i^{(m)}$ both have a negative energy (respectively $-\omega_{\text{at}}^{(n)}$ and $-\tilde{\omega}_m$). After linearization of the atomic dynamics it is possible to derive an exact non-Markovian Langevin equation for the photonic quantum field, by reexpressing the Hamiltonian dynamics into the form of Heisenberg equations

of motion for the various operators :

$$\partial_t a_i(t) = -i[a_i(t), H_{\text{ph}}(t)], \quad (4.11)$$

$$-i \sum_m g_m^* \hat{b}_i^{(m)}(t) - i\Omega_R \sum_k a_{\text{at},i}^{(n)\dagger}(t)$$

$$\partial_t a_{\text{at},i}^{(n)\dagger}(t) = -i\omega_{\text{at}} a_{\text{at},i}^{(n)\dagger}(t) + i \sum_m c_i^{(n,m)\dagger}(t), \quad (4.12)$$

$$+ i\Omega_R a_i(t)$$

$$\partial_t b_i^{(m)}(t) = -i\omega_m b_i^{(m)}(t) - i g_m a_i(t), \quad (4.13)$$

$$\partial_t c_i^{(n,m)\dagger}(t) = -i\tilde{\omega}_m c_i^{(n,m)\dagger}(t) - i\tilde{g}_m a_{\text{at},i}^{(n)\dagger}(t). \quad (4.14)$$

Injecting the integrated equation (4.14) for the bath oscillators into the equation (4.12) for the atomic degrees of freedom, we obtain a Markovian quantum Langevin equation for the atomic field coupled to the photonic field :

$$\partial_t a_{\text{at},i}^{(n)\dagger}(t) = \left(-i\omega_{\text{at}}^{(n)} - \frac{\Gamma_{\text{p}}^{\text{at}}}{2} \right) a_{\text{at},i}^{(n)\dagger}(t) + i\Omega_R a_i(t) + \hat{\xi}_{\text{at},i}^{(n)}(t) \quad (4.15)$$

with a Markovian quantum noise contribution related to atomic pumping :

$$\langle \hat{\xi}_{\text{at},i}^{(n)}(t+\tau) \hat{\xi}_{\text{at},i}^{(n')\dagger}(t) \rangle = \delta_{i,j} \delta_{n,n'} \Gamma_{\text{p}}^{\text{at}} \delta(\tau), \quad (4.16)$$

$$\langle \hat{\xi}_{\text{at},i}^{(n)\dagger}(t+\tau) \hat{\xi}_{\text{at},i}^{(n')}(t) \rangle = 0. \quad (4.17)$$

Then, integrating Eqs. (4.15), (4.13) and injecting them in Eq. (4.11) we get for the photonic dynamics :

$$\begin{aligned} \partial_t a_i(t) = & -i[a_i(t), H_{\text{ph}}(t)] - \int_{t'}^t \Gamma_1(t') a_i(t-t') + \hat{\xi}_{1,i}(t) \\ & + \int_0^t ds \left(\sum_n \Omega_R^2 e^{(-i\omega_{\text{at}}^{(n)} - \frac{\Gamma_{\text{p}}^{\text{at}}}{2})(t-s)} a_i(s) \right) \\ & - i\Omega_R \int_0^t ds \sum_n e^{(-i\omega_{\text{at}}^{(n)} - \frac{\Gamma_{\text{p}}^{\text{at}}}{2})(t-s)} \hat{\xi}_{\text{at},i}^{(n)}(s) \\ & - i\Omega_R e^{(-i\tilde{\omega}_m - \frac{\Gamma_{\text{p}}^{\text{at}}}{2})t} \sum_n a_{\text{at},i}^{(n)\dagger}(0), \end{aligned} \quad (4.18)$$

where the expressions for the loss memory kernel and noise autocorrelations are described below.

A. Langevin equation: general form

At long times with respect to $1/\Gamma_{\text{p}}^{\text{at}}$, the time-dependent contribution $\propto e^{(-i\tilde{\omega}_m - \frac{\Gamma_{\text{p}}^{\text{at}}}{2})t} \sum_n a_{\text{at},i}^{(n)\dagger}(0)$ in Eq. (4.18) (which represents a memory of the initial conditions) vanishes, and we can also replace the boundaries in the various integrals by 0 and $+\infty$. We obtain then the final form for the photonic non-Markovian Langevin equation of Eq. (2.1)

$$\begin{aligned} \partial_t \hat{a}_i(t) = & -i[\hat{a}_i(t), H_{\text{ph}}(t)] \\ & + \int_{-\infty}^{\infty} d\tau [\Gamma_{\text{p}}(\tau) - \Gamma_1(\tau)] \hat{a}_i(t-\tau) + \hat{\xi}_{\text{p},i}(t) + \hat{\xi}_{1,i}(t) \end{aligned} \quad (4.19)$$

where $\hat{\xi}_{\text{p},i}(t) = -i\Omega_R \int_{-\infty}^t ds \sum_n e^{(-i\omega_{\text{at}}^{(n)} - \frac{\Gamma_{\text{p}}^{\text{at}}}{2})(t-s)} \hat{\xi}_{\text{at},i}^{(n)}(s)$. The non-zero contributions for the two-points quantum noise autocorrelations can be summarized into :

$$\begin{aligned} \langle \hat{\xi}_{1,i}(t+\tau) \hat{\xi}_{1,j}^{\dagger}(t) \rangle &= \delta_{i,j} \int_{\omega} \mathcal{S}_1(\omega) e^{-i\omega\tau} \\ \langle \hat{\xi}_{\text{p},i}^{\dagger}(t+\tau) \hat{\xi}_{\text{p},j}(t) \rangle &= \delta_{i,j} \int_{\omega} \mathcal{S}_{\text{p}}(\omega) e^{+i\omega\tau} \end{aligned} \quad (4.20)$$

where $\Gamma_1(\tau) = \theta(\tau) \int_{\omega} \mathcal{S}_1(\omega) e^{-i\omega\tau}$ and $\Gamma_{\text{p}}(\tau) = \theta(\tau) \int_{\omega} \mathcal{S}_{\text{p}}(\omega) e^{-i\omega\tau}$. While the loss power spectrum $\mathcal{S}_1(\omega)$ is provided in Eq. (4.7), the photonic pump power spectrum has the expression

$$\mathcal{S}_{\text{p}}(\omega) = \Gamma_{\text{p}}^{\text{at}} \int d\omega' \mathcal{D}(\omega') \frac{(\Gamma_{\text{p}}^{\text{at}}/2)^2}{(\omega - \omega')^2 + (\Gamma_{\text{p}}^{\text{at}}/2)^2}, \quad (4.21)$$

with $\Gamma_{\text{p}}^{\text{at}} = \frac{4\Omega_R^2}{\Delta_{\text{diss}}}$: as in [33, 37], each atom is responsible for a Lorentzian contribution to photonic pumping, the continuous sum of the various contributions then provides the full spectrum $\mathcal{S}_{\text{p}}(\omega)$.

B. Some examples of realizable power spectra

1. First example: Markovian losses and Lorentzian pump power spectra

As a first example, we set ourselves in the configuration in which losses are Markovian processes, i.e., $\mathcal{S}_{\text{p}}(\omega) = \Gamma_1$, and all atomic transitions are equal to ω_{p} , in such a way that $\mathcal{D}(\omega) = N_{\text{at}} \delta(\omega - \omega_{\text{p}})$. In that case we obtain for the pump spectrum the Lorentzian form:

$$\mathcal{S}_{\text{p}}(\omega) = N_{\text{at}} \Gamma_{\text{p}}^{\text{at}} \frac{(\Delta_{\text{diss}}/2)^2}{(\omega - \omega_{\text{p}})^2 + (\Delta_{\text{diss}}/2)^2}, \quad (4.22)$$

where we have set the value $\Gamma_{\text{p}}^{\text{at}} = \Delta_{\text{diss}}$ for the atomic pumping rate. This configuration leads to the specific model Eq. (2.8) introduced in Sec. II that we have chosen in order to perform numerical simulations.

2. Second example: artificial Kennard-Stepanov relation

Another option would be to engineer non-trivial distributions $\mathcal{D}(\omega)$ (which we could imagine to do in a fictitious way by tuning all atoms to different frequencies, or by using several atomic species) of the atomic transition frequencies in such a way to simulate a Kennard-Stepanov relation. More specifically, we choose losses to be also Markovian $\mathcal{S}_1(\omega) = \Gamma_1$, and the particular form for the distribution of atomic transition frequencies:

$$\mathcal{D}(\omega) = \mathcal{D}_0 e^{\beta_{\text{eff}} \omega}. \quad (4.23)$$

In that case the pump power spectrum becomes

$$\mathcal{S}_{\text{p}}(\omega) = \mathcal{D}_0 \Gamma_{\text{p}}^{\text{at}} \int d\omega' e^{\beta_{\text{eff}} \omega'} \frac{(\Gamma_{\text{p}}^{\text{at}}/2)^2}{(\omega - \omega')^2 + (\Gamma_{\text{p}}^{\text{at}}/2)^2}. \quad (4.24)$$

In the limit of a very weak pumping rate $\Gamma_p^{\text{at}} \ll T_{\text{eff}} = 1/\beta_{\text{eff}}$, we recover the exponential-shaped spectrum:

$$S_p(\omega) = \Gamma_p e^{\beta_{\text{eff}} \omega}, \quad (4.25)$$

where $\Gamma_p = \frac{\pi}{2} \mathcal{D}_0 \Delta_{\text{diss}} \Gamma_p^{\text{at}}$. The Kennard-Stepanov relation Eq. (2.7) is thus reproduced artificially even though the photonic environment is highly out-of-equilibrium. Theoretically, this spectral shape (initially proposed in [36]) can be reproduced for an arbitrary low temperature: if necessary one can lower simultaneously the pumping rate $\Gamma_p^{\text{at}} = \Delta_{\text{diss}}$ and Ω_R , while increasing the number of atoms in order to stay within the previously described conditions of validity of the quantum Langevin equation (4.19). Concretely, for very low T_{eff} the engineering procedure might become more complex as it requires a high number of emitters with a fine control on transition frequencies.

C. Pseudo-thermalization in exciton-polaritons low-T experiments

The artificial Kennard-Stepanov configuration mentioned in Sec. IV B 2 might also be naturally reproduced in low-T exciton-polaritons experiments [8, 9]: while most theoretical works in the early literature [16, 17] have stressed on the impact of exciton-exciton scattering processes in the relaxation of polaritons into the bottleneck region of lower branch, more recent experimental observations [18] highlighted the important role played by high energy longitudinal optical (LO) phonons. It appears that in some regimes those processes even constitute the dominant relaxation channel for polaritons. Which discuss here what might be the implications regarding the nature of thermalization in such physical situation.

Since the excitons (located in a higher energy with respect to the bottom of the polaritonic band) usually undergo fast collisions/energy exchanges processes and also possess a much longer lifetime than polaritons, the exciton reservoir is rather well thermalized (while polaritons might not thermalize) and can thus be described by a classical Boltzmann distribution $n_X(\epsilon_k^X) \propto e^{-\beta \epsilon_k^X}$ (excitons being very massive particles, their degree of degeneracy is usually very weak in those experiments).

One hand, since the LO phonons dispersion law is typically very flat and strongly located around the frequency ω_{LO} (in stark contrast with acoustic phonons whose dispersion law present a light-cone structure), the LO phonon-assisted scattering processes excitons \rightarrow polaritons maintain the full information on the excitonic energy distribution and transfer it into the frequency-dependence of the polariton injection rate (up to an energy shift $\hbar\omega_{\text{LO}}$): in the hypothesis that LO phonon-assisted scattering processes are dominant, the polaritonic injection rate should thus present an exponential frequency dependence ($S_p(\omega) \simeq \Gamma_p^P e^{-\beta_{\text{eff}} \omega}$) at very a good degree of approximation. On the other hand, in that same picture, polariton \rightarrow exciton recombination processes are strongly inhibited as they would involve the absorption of a phonon from the LO phononic reservoir, which can be approximated as being close to the vacuum state (LO phonons possessing a sig-

nificantly higher energy ($\simeq 5 \text{ meV}$) than the typical temperatures ($\simeq 0.5 \text{ meV}$) in exciton-polaritons). As a consequence, polaritonic losses are by far dominated by mirror transparency effects, and can be well represented by Markovian processes: $S_l(\omega) \simeq \Gamma_l^P = x_{\text{ph}} \Gamma_{\text{ph}}$, where x_{ph} is the photonic fraction in the bottom of the lower polaritonic branch, and Γ_{ph} is the photonic loss rate. One concludes that the Kennard-Stepanov relation $S_p(\omega)/S_l(\omega) \simeq \Gamma_p^P/\Gamma_l^P e^{-\beta_{\text{eff}} \omega}$ might be artificially verified in that context (at least in a broad frequency region), and polaritons be subject to pseudo-thermalization.

The measurement of thermal signatures in those experiments has thus to be interpreted carefully. In that prospect, it might be interesting to verify that polaritons are indeed equilibrated with excitons (i.e., their environment) in order to provide conclusions regarding a true thermalization or a pseudo-thermalization: one way to proceed would be to check the validity of the FDT associated to a pair of operators $\hat{A}(t)$ and $\hat{B}(t)$ (with the notations of Sec. III B) associated respectively to polariton and exciton degrees of freedoms, by measuring the corresponding frequency-dependent effective temperature.

V. HOW TO BREAK PSEUDO-THERMALIZATION

Expectedly, the low-energy pseudo-thermalization effect described in Sec. III is not a fully general properties of driven-dissipative quantum systems, since a wide class of models can not been cast into the form of the quantum Langevin Eq. (2.1) which only implements non-Markovian effects. In this section, we discuss a simple extension of Eq. (2.1) which allows to break the emergent equilibrium presented in Sec. III. More specifically, we introduce a generalized Bogoliubov-de Gennes model at low energies and low momenta, with a complex kinetic energy and a complex chemical potential:

$$-i\omega \hat{\Lambda}_{\mathbf{k}}(\omega) = -i \left[z \epsilon_{\mathbf{k}} \hat{\Lambda}_{\mathbf{k}}(\omega) + \tilde{z} \mu \left(\hat{\Lambda}_{\mathbf{k}}(\omega) + \hat{\Lambda}_{-\mathbf{k}}^\dagger(-\omega) \right) \right] + \hat{\xi}_{\text{neq},\mathbf{k}}(\omega). \quad (5.1)$$

The noise auto correlation is

$$\begin{aligned} \langle \hat{\xi}_{\text{neq},\mathbf{k}}(\omega) \hat{\xi}_{\text{neq},\mathbf{k}'}^\dagger(\omega') \rangle &= \langle \hat{\xi}_{\text{neq},\mathbf{k}}^\dagger(\omega) \hat{\xi}_{\text{neq},\mathbf{k}}(\omega') \rangle \\ &= \delta_{\mathbf{k}-\mathbf{k}'} \delta_{\omega-\omega'} S_l(\omega_{\text{BEC}}), \end{aligned} \quad (5.2)$$

and complex couplings are written in phase-modulus representation as $z = \rho e^{-i\theta}$, $\tilde{z} = \tilde{\rho} e^{-i\tilde{\theta}}$. This model is very similar to the low-energy model Eq. (2.28) derived in a previous section, except that the kinetic energy ϵ_k and the chemical potential μ have respectively been multiplied by two different complex numbers z and \tilde{z} (while they were multiplied by the same complex in the low-energy theory Eq. (2.28)). In Sec. V A and Sec. V B we will show that in case of alignment in the complex plane of these couplings (i.e., $\theta = \tilde{\theta}$), we obtain an effective equilibrium theory, while in the case of a misalignment, the steady state presents non-equilibrium features. Finally in Sec. V C, we will describe many ways to implement those modified complex couplings.

A. Static correlations

Analysing Eqs. (5.1),(5.2) we obtain the following expression for momentum distribution $n_k^{neq} = \langle \hat{\Lambda}_{\mathbf{k}}^\dagger \hat{\Lambda}_{\mathbf{k}} \rangle$ and the anomalous average $\mathcal{A}_k^{neq} = \langle \hat{\Lambda}_{\mathbf{k}} \hat{\Lambda}_{-\mathbf{k}} \rangle$ (the derivation is very similar to the one made in App. VII B):

$$n_k^{neq} = \frac{|z\epsilon_k + \tilde{z}\mu|^2 S_1(\omega_{\text{BEC}})/2}{(\rho \sin(\theta)\epsilon_k + \tilde{\rho} \sin(\tilde{\theta})\mu) \rho \epsilon_k (\rho \epsilon_k + 2\cos(\theta - \tilde{\theta})\tilde{\rho}\mu)}, \quad (5.3)$$

$$\mathcal{A}_k^{neq} = \frac{-(z^*\epsilon_k + \tilde{z}^*\mu)\tilde{z}\mu S_1(\omega_{\text{BEC}})/2}{(\rho \sin(\theta)\epsilon_k + \tilde{\rho} \sin(\tilde{\theta})\mu) \rho \epsilon_k (\rho \epsilon_k + 2\cos(\theta - \tilde{\theta})\tilde{\rho}\mu)}. \quad (5.4)$$

In the general case, it is not possible to further simplify those expression, and the steady-state properties differs from the equilibrium statistics. However, considering the particular case in which the complex couplings z and \tilde{z} are aligned in the complex plane, i.e., $\theta = \tilde{\theta}$, one obtains

$$n_k^{\text{aligned}} = \frac{\tilde{T}_{\text{eff}}(\rho\epsilon_k + \tilde{\rho}\mu)}{\rho\epsilon_k(\rho\epsilon_k + 2\tilde{\rho}\mu)}, \quad (5.5)$$

$$\mathcal{A}_k^{\text{aligned}} = \frac{-\tilde{T}_{\text{eff}}\tilde{\rho}\mu}{\rho\epsilon_k(\rho\epsilon_k + 2\tilde{\rho}\mu)}, \quad (5.6)$$

which compared to Eqs. (3.3), (3.4), corresponds to a low-energy effective equilibrium statistics with $\tilde{T}_{\text{eff}} = \frac{S_1(\omega_{\text{BEC}})}{2\sin(\theta)}$ and renormalized couplings $\epsilon_k \rightarrow \rho\epsilon_k$, $\mu \rightarrow \tilde{\rho}\mu$. This is not surprising since in that case, the generalized Bogoliubov-de Gennes model given by Eq. (5.1) coincides with the low frequency limit Eq. (2.28) of the non-Markovian Langevin equation studied in this paper. We conclude that the alignment configuration of the couplings z and \tilde{z} of Eq. (2.28) corresponds to an effective equilibrium situation, while the general case of non-alignment drives the system out-of-equilibrium, as thoroughly discussed in [26, 27, 29].

Although Eqs. (5.3), (5.4) present deviations from the Rayleigh-Jeans thermal laws $n_k \xrightarrow{E_k \rightarrow 0} \frac{T_{\text{eff}}(\epsilon_k + \mu)}{E_k^2}$, for a generic choice misalignment of z and \tilde{z} the low-momentum correlations still present a $\frac{1}{k^2}$ equilibrium-like infrared divergence (and we do not expect any particular loss of coherence by driving the system out-of-equilibrium, at least in three dimensions), apart for one specific pathological configuration: if we put ourselves in the specific configuration in which we set the phase θ to 0 and the phase $\tilde{\theta}$ to $\pi/2$, which can be obtained by using Markovian baths, cancelling the photon-photon interactions and adding saturation to the pump (see Sec. V C 2), we indeed obtain a very different behaviour

$$n_k^{\text{pathological}} = \frac{S_1(\omega_{\text{BEC}})(\epsilon_k^2 + (\tilde{\rho}\mu)^2)}{2\tilde{\rho}\mu\epsilon_k^2}, \quad (5.7)$$

$$\mathcal{A}_k^{\text{pathological}} = \frac{iS_1(\omega_{\text{BEC}})(\epsilon_k + i\tilde{\rho}\mu)\tilde{\rho}\mu}{2\tilde{\rho}\mu\epsilon_k^2}. \quad (5.8)$$

We see that the momentum distribution changes behaviour at long range : $n(k) \simeq \frac{1}{k^4}$, such a features has already been predicted in [21].

Due to these increased low-momenta fluctuations, we might be tempted to conclude that in three dimensions, a non-equilibrium free Bose gas in presence of a pump and saturation, i.e., a 3D VCSEL [44] can not Bose-condense (while the equilibrium free Bose gas is known to condense). However, in this case the Bogoliubov approach is ill-defined and can not be applied in a straightforward manner. Instead, studying the long range properties of this system requires applying the renormalization group methods to this non-equilibrium system keeping all non-linearities (and thus the ones providing from saturation): our understanding is that during the RG flow [26, 27], a small photon-photon interaction should be generated and the true correlations should be thus in $n(k) \simeq \frac{1}{k^2}$, saving thus the convergence. Such effect was verified numerically in [52] by simulating the Kardar-Parisi-Zhang equation (however in that case the simulations were done in a 1D configuration).

B. Momentum-dependent effective temperatures from FDT

It is also interesting to check whether a misalignment of the couplings affects the validity of the FDT. To do so, we will use an exact model providing a quantum Langevin equation valid at all frequencies which leads at low-frequencies and low-momenta to the effective description Eq. (5.1) with non-aligned couplings z and \tilde{z} : this model is defined in the next section in Eqs (5.9), (5.12). We computed the corresponding effective temperatures $\beta_{1,\text{eff}}(\mathbf{k}, \omega)$ and $\beta_{2,\text{eff}}(\mathbf{k}, \omega)$ by mean of the definitions Eqs (3.24). In Fig. 7, we show $\beta_{1,\text{eff}}(\mathbf{k}, \omega)$ (resp. $\beta_{2,\text{eff}}(\mathbf{k}, \omega)$) in the left panel (resp. right panel) in function ω in units of Δ_{diss} for various momenta \mathbf{k} : we notice that in the region $\omega \ll \Delta_{\text{diss}}$, these effective temperatures do not take anymore identical values, so the low-frequency temperatures are momentum dependent. We conclude that pseudo-thermalization is broken not only at a static level (in the sense that it does not respect perfectly the Rayleigh-Jeans law obtained for a weakly interacting isolated Bose gas) in case of misalignment, but also at a dynamical level, as the FDT is not verified at low-frequencies. We remark that at low momenta, the zero-frequency effective inverse temperatures progressively converge toward the value β_{eff} predicted in Secs. III A 1, III B.

C. Examples of modified quantum optics models driving the system out-of-equilibrium

In this section, we discuss various physical ways to obtain the modified Bogoliubov-de Gennes system Eq. (5.1) with misalignment of the complex couplings, by mean of simple modifications with respect to the quantum optics model introduced in Sec. IV.

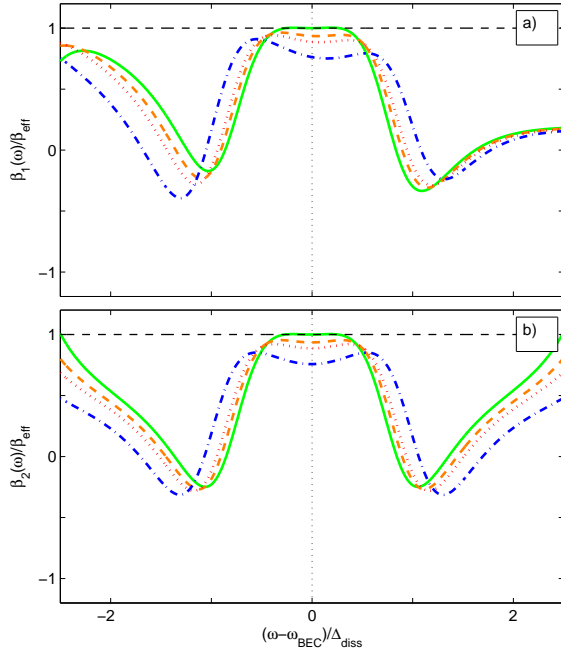


Figure 7: Test of the FDT/KMS relation in the presence of dispersion of the emitters. Panel a) (resp. b)): frequency-dependent effective temperature $\beta_{1,\text{eff}}(\mathbf{k}, \omega)$ (resp. $\beta_{2,\text{eff}}(\mathbf{k}, \omega)$) defined in Eq. (2.5) for a Lorentzian pump, massive emitters and Markovian losses (model defined in Sec.V C 1), in function of the frequency $\omega - \omega_{\text{BEC}}$ in units of Δ_{diss} , and for various momenta \mathbf{k} . Parameters: $m = 1$, $M_{\text{at}} = 3$, $\Gamma_l/\Gamma_p^0 = 0.3$, $\Gamma_p/\Delta_{\text{diss}} = 0.01$, $\delta/\Delta_{\text{diss}} = -2$. For each panel, the various curves corresponds to increasing momenta \mathbf{k} (chosen in such a way that the corresponding Bogoliubov spectrum spans all energy above and below the resulting effective temperature $T_{\text{eff}}^{\text{disp}} \equiv 1/\beta_{\text{eff}}^{\text{disp}} = 0.54\Delta_{\text{diss}}$): $k/k_{\text{th}} = 0.18$ for the green solid line, $k/k_{\text{th}} = 3.65$, for the orange dashed line, $k/k_{\text{th}} = 9.1$ for the red dotted line, $k/k_{\text{th}} = 54.7$ for the dash-dotted blue line: $k/k_{\text{th}} = 3 \times 10^{-2}$ for the green solid line, $k/k_{\text{th}} = 1.83$, for the orange dashed line, $k/k_{\text{th}} = 2.43$ for the red dotted line, $k/k_{\text{th}} = 3.66$ for the dash-dotted blue line. Here k_{th} is also defined by $E(\mathbf{k}_{\text{th}}) = T_{\text{eff}}^{\text{disp}}$

1. Emitters with dispersion

The first model we introduce is very similar to the one presented in Sec. II, except that we add a momentum-dependence to the pump: in the photonic case presented in Sec. IV, this can be obtained taking into account the dispersion relation for the emitters which can be two-level massive atoms, and the recoil energy during injection of a photon. We obtain the following Langevin equation:

$$\frac{\partial}{\partial t} \hat{\psi}_{\mathbf{k}}(t) = -i [\hat{\psi}_{\mathbf{k}}(t), H_{\text{ph}}(t)] + \int_{-\infty}^{\infty} d\tau [\Gamma_{p,\mathbf{k}}(\tau) - \Gamma_l(\tau)] \hat{\psi}_{\mathbf{k}}(t - \tau) + \hat{\xi}_{\text{disp},\mathbf{k}}(t), \quad (5.9)$$

with the non-Markovian momentum-dependent dissipative kernel for pumping

$$\Gamma_{p,\mathbf{k}}(\tau) = \Theta(\tau) \int_{\omega} S_{p,\mathbf{k}}(\omega) e^{-i\omega\tau}, \quad (5.10)$$

and noise correlations in momentum-frequency space

$$\langle \hat{\xi}_{\text{disp},\mathbf{k}}(\omega) \hat{\xi}_{\text{disp},\mathbf{k}'}^{\dagger}(\omega') \rangle = \delta_{\mathbf{k}-\mathbf{k}'} \delta_{\omega-\omega'} S_l(\omega_{\text{BEC}} + \omega), \quad (5.11a)$$

$$\langle \hat{\xi}_{\text{disp},\mathbf{k}}^{\dagger}(\omega) \hat{\xi}_{\text{disp},\mathbf{k}'}(\omega') \rangle = \delta_{\mathbf{k}-\mathbf{k}'} \delta_{\omega-\omega'} S_{p,\mathbf{k}}(\omega_{\text{BEC}} + \omega). \quad (5.11b)$$

The pump power spectrum depends now not only on the frequency but also on the momentum. To test the FDT, we use the full non-Markovian theory Eq. (5.9), and apply the Bogoliubov procedure to calculate analytically the correlation functions. We choose the specific form for the momentum-frequency dependent pump power spectrum:

$$S_{p,\mathbf{k}}(\omega) = \Gamma_p \frac{(\Delta_{\text{diss}}/2)^2}{(\omega + \epsilon_{\mathbf{k}}^p - \omega_p)^2 + (\Delta_{\text{diss}}/2)^2}. \quad (5.12)$$

This model takes into account the transition frequency of the emitters, shifted by the recoil energy $\epsilon_{\mathbf{k}}^p = \frac{k^2}{2M_p}$ of the emitters. If the mass M_p of the emitter is small enough, this effect can be physically relevant at high momenta.

From Eq. (5.9), applying a Bogoliubov procedure similarly to Sec. II D, we can derive a low-energy and low-momentum effective theory, as we did in Sec. II F:

$$-i\omega \hat{\Lambda}_{\mathbf{k}}(\omega) = -i \left[z_{\text{disp}} \epsilon_{\mathbf{k}} \hat{\Lambda}_{\mathbf{k}}(\omega) + \tilde{z}_{\text{disp}} \mu \left(\hat{\Lambda}_{\mathbf{k}}(\omega) + \hat{\Lambda}_{-\mathbf{k}}^{\dagger}(-\omega) \right) \right] + \bar{\xi}_{\text{disp},\mathbf{k}}(\omega). \quad (5.13)$$

The noise correlations are

$$\langle \bar{\xi}_{\text{disp},\mathbf{k}}(\omega) \bar{\xi}_{\text{disp},\mathbf{k}'}^{\dagger}(\omega') \rangle = \delta_{\mathbf{k}-\mathbf{k}'} \delta_{\omega-\omega'} S_l(\omega_{\text{BEC}}), \quad (5.14a)$$

$$\langle \bar{\xi}_{\text{disp},\mathbf{k}}^{\dagger}(\omega) \bar{\xi}_{\text{disp},\mathbf{k}'}(\omega') \rangle = \delta_{\mathbf{k}-\mathbf{k}'} \delta_{\omega-\omega'} S_{p,0}(\omega_{\text{BEC}}), \quad (5.14b)$$

where $S_{p,0}(\omega_{\text{BEC}}) = S_l(\omega_{\text{BEC}})$ and the complex couplings are

$$z_{\text{disp}} = (1 + \tilde{\delta} - i\tilde{\Gamma})(1 + 2im \underbrace{\partial_k^2 \Gamma_p|_{k=0, \omega=\omega_{\text{BEC}}}}_{<0}), \quad (5.15)$$

$$\tilde{z}_{\text{disp}} = (1 + \tilde{\delta} - i\tilde{\Gamma}). \quad (5.16)$$

We obtain some effective complex kinetic energy and chemical potential for the photonic dynamic. However, due to the dispersion of the emitters, an additional multiplicative contribution has been added to the complex kinetic energy inducing thus a misalignment between z_{disp} and \tilde{z}_{disp} . In order to test the validity of the fluctuation-dissipation theorem we define for this specific model $\beta_{\text{eff}} \equiv$

$$\frac{d}{d\omega} \log \left[\frac{S_l(\omega)}{S_{\text{em},k}(\omega)} \right] \Big|_{\omega=\omega_{\text{BEC}}, k=0}.$$

2. Saturation of the pump/two-body losses

In the second model, we propose to add saturation of the pump or two-body losses. Basing ourselves, on the photonic case presented in Sec. IV, some saturation stems from the fact that the emitters are two-level atoms and thus are not perfectly linear systems. In this case, at a qualitative level the Langevin equation for the quantum fluctuations becomes at low frequency:

$$-i\omega\hat{\Lambda}_{\mathbf{k}}(\omega) = -i\left[z_{sat}\epsilon_k\hat{\Lambda}_{\mathbf{k}}(\omega) + \tilde{z}_{sat}\mu\left(\hat{\Lambda}_{\mathbf{k}}(\omega) + \hat{\Lambda}_{-\mathbf{k}}^\dagger(-\omega)\right)\right] + \bar{\xi}_{sat,\mathbf{k}}(\omega). \quad (5.17)$$

The noise correlations are

$$\langle\bar{\xi}_{sat,\mathbf{k}}(\omega)\bar{\xi}_{sat,\mathbf{k}'}^\dagger(\omega')\rangle = \delta_{\mathbf{k}-\mathbf{k}'}\delta_{\omega-\omega'}S_l(\omega_{\text{BEC}}), \quad (5.18a)$$

$$\langle\bar{\xi}_{sat,\mathbf{k}}^\dagger(\omega)\bar{\xi}_{sat,\mathbf{k}'}(\omega')\rangle = \delta_{\mathbf{k}-\mathbf{k}'}\delta_{\omega-\omega'}S_l(\omega_{\text{BEC}}), \quad (5.18b)$$

and the complex couplings are

$$z_{sat} = (1 + \tilde{\delta} - i\tilde{\Gamma}), \quad (5.19)$$

$$\tilde{z}_{sat} = (1 + \tilde{\delta} - i\tilde{\Gamma})(1 - i\gamma_{sat}). \quad (5.20)$$

γ_{sat} is a dimensionless coupling quantifying the saturation effect, i.e., an increase of the dissipation strength with the density $\hat{\Lambda}_{\mathbf{k}}^\dagger\hat{\Lambda}_{\mathbf{k}}$, which linearized gives in the Bogoliubov approach a complex contribution proportional to $\hat{\Lambda}_{\mathbf{k}} + \hat{\Lambda}_{-\mathbf{k}}^\dagger$. Here again, because of saturation which multiplies the chemical potential by some complex, we also observe a misalignment between z_{sat} and \tilde{z}_{sat} . We comment also that in presence of saturation, the noise should present non trivial non-linear autocorrelations depending on the quantum field $\hat{\Lambda}_{\mathbf{k}}$, but for the sake of simplicity we assumed it to be Gaussian as a first level of approximation.

VI. CONCLUSION AND PERSPECTIVES

In this work we have analysed the *pseudo-thermalization* effect, where an open quantum system coupled to several non-thermal and non-Markovian reservoirs presents an emergent thermal behavior in spite of the highly non-thermal nature of its environment. Our approach was based on a quantum Langevin formalism which allows us to overcome the inherent issues related to the quantum master equation formalism and the quantum regression theorem in a non-Markovian context, and then to compute arbitrary multiple time correlators. The focus was set on the exactly solvable case of a driven-dissipative weakly interacting Bose-Einstein Condensate.

In particular, we have shown that pseudo-thermalization not only occurs at the static level but is also accompanied by the satisfaction of the fluctuation-dissipation theorem at the dynamical level. According to the spectral properties of the chosen reservoirs, equilibrium signatures can be observed either only at low energies or globally. In the latter situation, which might be relevant in some exciton-polariton experiments,

the steady-state properties are completely undistinguishable from an equilibrium one. Finally, several modifications of the initial model allowing to break this pseudo-thermalization effect have been discussed, with a particular stress on the role played by the dispersion and the saturation of the emitters.

The results of this work challenge the common idea that only open quantum systems in contact with an equilibrated environment can behave completely thermally. It implies in particular that, before concluding to an equilibration, an experimentalist should check the thermal character not only of the system correlations, but also of the crossed correlations involving altogether the degrees of freedom of the system and the various reservoirs.

While this pseudo-thermalization is expected to be very robust and universal in the case where the Kennard-Stepanov relation is fully verified, it is unclear whether low-energy pseudo-thermalization should apply to generic physical systems for a typical choice of non-Markovian reservoirs: future studies will be dedicated in particular to the interplay between pseudo-thermalization and the departure of the Bogoliubov regime.

Acknowledgments

Discussions with Maxime Richard, Andrea Gambassi and Jamir Marino are warmly acknowledged. JL and IC are supported by the EU-FET Proactive grant AQuS, Project No. 640800, and by the Autonomous Province of Trento, partially through the project ‘‘On silicon chip quantum optics for quantum computing and secure communications’’ (‘‘SiQuro’’). A. C. acknowledges funding by the European Research Council via ERC Grant Agreement n. 647434 (DOQS).

VII. APPENDIX

A. Quantum correlations in frequency and FDT

In this Appendix, we compute the correlation matrix in momentum frequency space $C_{\mathbf{k}}(\omega)$ defined in Eq. (2.26). We then move to the calculation of the momentum-frequency-dependent effective inverse temperatures involved in the test of the validity of the FDT, and defined in Eqs. (3.24),(3.25). Inverting the Langevin equation in frequency space Eq.(2.23), we get :

$$\begin{pmatrix} \hat{\Lambda}_{\mathbf{k}}(\omega) \\ \hat{\Lambda}_{-\mathbf{k}}^\dagger(-\omega) \end{pmatrix} = \frac{i}{\omega - \mathcal{L}_{\mathbf{k}}(\omega)} \begin{pmatrix} \tilde{\xi}_{\mathbf{k}}(\omega) \\ -\tilde{\xi}_{-\mathbf{k}}^\dagger(-\omega) \end{pmatrix} \quad (7.1)$$

After calculation this gives us :

$$\begin{pmatrix} \hat{\Lambda}_{\mathbf{k}}(\omega) \\ \hat{\Lambda}_{-\mathbf{k}}^\dagger(-\omega) \end{pmatrix} = \frac{i}{\left[\omega - (\epsilon_{\mathbf{k}} + \mu + i\tilde{\Gamma}(\omega)) \right] \times \left[\omega + \epsilon_{\mathbf{k}} + \mu - i\tilde{\Gamma}^*(-\omega) \right] + \mu^2} \begin{pmatrix} (\omega + \epsilon_{\mathbf{k}} + \mu - i\tilde{\Gamma}^*(-\omega)) \tilde{\xi}_{\mathbf{k}}(\omega) - \mu \tilde{\xi}_{-\mathbf{k}}^\dagger(-\omega) \\ -\mu \tilde{\xi}_{\mathbf{k}}(\omega) + (-\omega + \epsilon_{\mathbf{k}} + \mu + i\tilde{\Gamma}(\omega)) \tilde{\xi}_{-\mathbf{k}}^\dagger(-\omega) \end{pmatrix}, \quad (7.2)$$

and taking the hermitian conjugate:

$$\begin{pmatrix} \hat{\Lambda}_{\mathbf{k}}^\dagger(\omega) \\ \hat{\Lambda}_{-\mathbf{k}}(-\omega) \end{pmatrix} = \frac{-i}{\left[\omega - (\epsilon_{\mathbf{k}} + \mu - i\tilde{\Gamma}^*(\omega)) \right] \times \left[\omega + \epsilon_{\mathbf{k}} + \mu + i\tilde{\Gamma}(-\omega) \right] + \mu^2} \begin{pmatrix} (\omega + \epsilon_{\mathbf{k}} + \mu + i\tilde{\Gamma}(-\omega)) \tilde{\xi}_{\mathbf{k}}^\dagger(\omega) - \mu \tilde{\xi}_{-\mathbf{k}}(-\omega) \\ -\mu \tilde{\xi}_{\mathbf{k}}^\dagger(\omega) + (-\omega + \epsilon_{\mathbf{k}} + \mu - i\tilde{\Gamma}^*(\omega)) \tilde{\xi}_{-\mathbf{k}}(-\omega) \end{pmatrix}. \quad (7.3)$$

We get after tracing over the various baths the expression for the correlation matrix:

$$C_{\mathbf{k}}(\omega) = \frac{1}{N_{\mathbf{k}}(\omega)N_{-\mathbf{k}}(-\omega)} \underbrace{\begin{pmatrix} M_{\mathbf{k}}^{(11)}(\omega) & M_{\mathbf{k}}^{(12)}(\omega) \\ M_{\mathbf{k}}^{(21)}(\omega) & M_{\mathbf{k}}^{(22)}(\omega) \end{pmatrix}}_{\equiv \mathcal{M}(\omega)}, \quad (7.4)$$

where

$$N_{\mathbf{k}}(\omega) = \left[\omega - (\epsilon_{\mathbf{k}} + \mu + i\tilde{\Gamma}(\omega)) \right] \times \left[\omega + \epsilon_{\mathbf{k}} + \mu - i\tilde{\Gamma}^*(-\omega) \right] + \mu^2 \quad (7.5a)$$

$$M_{\mathbf{k}}^{(11)}(\omega) = S_l(\omega_{BEC} + \omega) \left| \omega + \epsilon_{\mathbf{k}} + \mu + i\tilde{\Gamma}(-\omega) \right|^2 + S_p(\omega_{BEC} - \omega) \mu^2, \quad (7.5b)$$

$$M_{\mathbf{k}}^{(21)}(\omega) = -S_l(\omega_{BEC} + \omega) \times \left[\omega + \epsilon_{\mathbf{k}} + \mu + i\tilde{\Gamma}(-\omega) \right] \mu + S_p(\omega_{BEC} - \omega) \left[\omega - (\epsilon_{\mathbf{k}} + \mu + i\tilde{\Gamma}(\omega)) \right] \mu, \quad (7.5c)$$

$$M_{\mathbf{k}}^{(12)}(\omega) = -S_l(\omega_{BEC} + \omega) \times \left[\omega + \epsilon_{\mathbf{k}} + \mu - i\tilde{\Gamma}^*(-\omega) \right] \mu + S_p(\omega_{BEC} - \omega) \left[\omega - (\epsilon_{\mathbf{k}} + \mu - i\tilde{\Gamma}^*(\omega)) \right] \mu, \quad (7.5d)$$

$$M_{\mathbf{k}}^{(22)}(\omega) = S_l(\omega_{BEC} + \omega) \mu^2 + S_p(\omega_{BEC} - \omega) \times \left| \omega - (\epsilon_{\mathbf{k}} + \mu + i\tilde{\Gamma}(\omega)) \right|^2. \quad (7.5e)$$

To test the FDT it is also useful to calculate the ratios $\frac{\langle \hat{\Lambda}_{\mathbf{k}}(\omega) \hat{\Lambda}_{\mathbf{k}}^\dagger \rangle}{\langle \hat{\Lambda}_{\mathbf{k}}^\dagger(\omega) \hat{\Lambda}_{\mathbf{k}} \rangle}$ and $\frac{\langle \hat{\Lambda}_{\mathbf{k}}(\omega) \hat{\Lambda}_{-\mathbf{k}} \rangle}{\langle \hat{\Lambda}_{\mathbf{k}}(-\omega) \hat{\Lambda}_{-\mathbf{k}} \rangle}$. We obtain the following expres-

sions:

$$\frac{\langle \hat{\Lambda}_{\mathbf{k}}(\omega) \hat{\Lambda}_{\mathbf{k}}^\dagger \rangle}{\langle \hat{\Lambda}_{\mathbf{k}}^\dagger(\omega) \hat{\Lambda}_{\mathbf{k}} \rangle} = \frac{S_l(\omega_{BEC} + \omega) + S_p(\omega_{BEC} - \omega) A_{\mathbf{k}}(\omega)}{S_p(\omega_{BEC} + \omega) + S_l(\omega_{BEC} - \omega) A_{\mathbf{k}}(\omega)}, \quad (7.6)$$

$$\frac{\langle \hat{\Lambda}_{\mathbf{k}}(\omega) \hat{\Lambda}_{-\mathbf{k}} \rangle}{\langle \hat{\Lambda}_{\mathbf{k}}(-\omega) \hat{\Lambda}_{-\mathbf{k}} \rangle} = \frac{S_l(\omega_{BEC} + \omega) + S_p(\omega_{BEC} - \omega) B_{\mathbf{k}}(\omega)}{S_p(\omega_{BEC} + \omega) + S_l(\omega_{BEC} - \omega) B_{\mathbf{k}}(\omega)}, \quad (7.7)$$

with

$$A_{\mathbf{k}}(\omega) = \frac{\mu^2}{\left| \omega + \epsilon_{\mathbf{k}} + \mu + i\tilde{\Gamma}(-\omega) \right|^2}, \quad (7.8)$$

$$B_{\mathbf{k}}(\omega) = \frac{-\omega + \epsilon_{\mathbf{k}} + \mu - i\tilde{\Gamma}^*(\omega)}{\omega + \epsilon_{\mathbf{k}} + \mu - i\tilde{\Gamma}^*(-\omega)}. \quad (7.9)$$

B. Static correlations at low energy

In this Appendix, we calculate the static correlations at steady state in the low-energy regime $E_{\mathbf{k}} \ll \Delta_{\text{diss}}$. In this regime, using the definition Eq. (2.29) as well as the fact that $S_l(\omega_{BEC}) = S_p(\omega_{BEC})$, we can approximate the expression Eq. (7.4) of the correlation matrix calculated in the previous Appendix as:

$$\begin{aligned} N_{\mathbf{k}}(\omega) &\simeq \frac{1}{|z|^2} \{ [\omega - z(\epsilon_{\mathbf{k}} + \mu)] [\omega + z^*(\epsilon_{\mathbf{k}} + \mu)] + |z|^2 \mu^2 \} \\ &= \frac{1}{|z|^2} (\omega - \omega_{\mathbf{k}}^+) (\omega - \omega_{\mathbf{k}}^-), \end{aligned} \quad (7.10a)$$

$$M_{\mathbf{k}}^{(11)}(\omega) \simeq \frac{S_l(\omega_{BEC})}{|z|^2} [|\omega + z(\epsilon_{\mathbf{k}} + \mu)|^2 + |z|^2 \mu^2], \quad (7.10b)$$

$$M_{\mathbf{k}}^{(21)}(\omega) \simeq -2S_l(\omega_{BEC})(\epsilon_{\mathbf{k}} + \mu)\mu, \quad (7.10c)$$

$$M_{\mathbf{k}}^{(12)}(\omega) \simeq -2S_l(\omega_{BEC})(\epsilon_{\mathbf{k}} + \mu)\mu, \quad (7.10d)$$

$$M_{\mathbf{k}}^{(22)}(\omega) \simeq \frac{S_l(\omega_{BEC})}{|z|^2} [|\omega - z(\epsilon_{\mathbf{k}} + \mu)|^2 + |z|^2 \mu^2], \quad (7.10e)$$

where $\omega_{\mathbf{k}}^\pm$ are the complex low energy mode frequencies of the condensate given by Eq. (2.31). From these expressions, we can calculate the dynamic structure factor $\mathcal{S}_{\mathbf{k}}(t)$, which is defined as

$$\mathcal{S}_{\mathbf{k}}(t) = \begin{pmatrix} \langle \hat{\Lambda}_{\mathbf{k}}(t) \hat{\Lambda}_{\mathbf{k}}^\dagger(0) \rangle & \langle \hat{\Lambda}_{\mathbf{k}}(t) \hat{\Lambda}_{-\mathbf{k}}(0) \rangle \\ \langle \hat{\Lambda}_{-\mathbf{k}}^\dagger(t) \hat{\Lambda}_{\mathbf{k}}^\dagger(0) \rangle & \langle \hat{\Lambda}_{-\mathbf{k}}^\dagger(t) \hat{\Lambda}_{-\mathbf{k}}(0) \rangle \end{pmatrix}, \quad (7.11)$$

and is related to the correlation matrix $C_{\mathbf{k}}(\omega)$ as $\int_t \mathcal{S}_{\mathbf{k}}(t) e^{-i\omega t} = C_{\mathbf{k}}(\omega)$. Using a pole integration in the complex plane we obtain

$$\mathcal{S}_{\mathbf{k}}(t) = \frac{-i|z|^2}{2(\omega_{\mathbf{k}}^+ - \omega_{\mathbf{k}}^-)(\omega_{\mathbf{k}}^+ + \omega_{\mathbf{k}}^-)} \left[\frac{\mathcal{M}(\omega_{\mathbf{k}}^+) e^{-i\omega_{\mathbf{k}}^+ t}}{2\omega_{\mathbf{k}}^+} - \frac{\mathcal{M}(\omega_{\mathbf{k}}^-) e^{-i\omega_{\mathbf{k}}^- t}}{\omega_{\mathbf{k}}^-} \right], \quad (7.12)$$

where $\mathcal{M}(\omega)$ has been defined in Eq. (7.4). Setting $t = 0$ we find the static correlation matrix :

$$S_{\mathbf{k}}(0) = \frac{-i|z|^2}{2(\omega_{\mathbf{k}}^+ - \omega_{\mathbf{k}}^-)(\omega_{\mathbf{k}}^+ + \omega_{\mathbf{k}}^-)} \left[\frac{\mathcal{M}(\omega_{\mathbf{k}}^+)}{2\omega_{\mathbf{k}}^+} - \frac{\mathcal{M}(\omega_{\mathbf{k}}^-)}{\omega_{\mathbf{k}}^-} \right]. \quad (7.13)$$

By injecting the expressions given by Eqs. (7.10) as well as the explicit expressions for the condensate frequencies Eq. (2.31), we find:

$$S_{\mathbf{k}}(0) = \frac{S_1(\omega_{BEC})|z|^2}{2z_I E_k^2} \begin{pmatrix} \epsilon_k + \mu & -\mu \\ -\mu & \epsilon_k + \mu \end{pmatrix}. \quad (7.14)$$

From Eqs. (2.29), (2.5), we have that $\frac{z_I}{|z|^2} = \text{Im}(z^{-1}) = -\frac{d\text{Re}(\tilde{\Gamma}(\omega))}{d\omega} \Big|_{\omega=0} = \frac{\beta_{\text{eff}} S_1(\omega_{BEC})}{2}$, from which we deduce the final expression:

$$S_{\mathbf{k}}(0) = \frac{T_{\text{eff}}}{E_k^2} \begin{pmatrix} \epsilon_k + \mu & -\mu \\ -\mu & \epsilon_k + \mu \end{pmatrix}. \quad (7.15)$$

References

-
- [1] I. Carusotto and C. Ciuti, Rev. Mod. Phys. **85**, 299 (2013).
 - [2] M. J. Hartmann, J. Opt. **18**, 104005 (2016).
 - [3] S. Diehl, A. Micheli, A. Kantian, B. Kraus, H. P. Büchler and P. Zoller, Nat. Phys. **4**, 878 (2008).
 - [4] R. P. Feynman and F. L. Vernon Jr., Ann. Phys. **24**, 118 (1963).
 - [5] A. Caldeira and A. J. Leggett, Phys. Rev. Lett. **46**, 211 (1981).
 - [6] H.-P. Breuer and F. Petruccione, *The theory of open quantum systems* (Clarendon Press, Oxford, 2006).
 - [7] C. W. Gardiner and P. Zoller, *Quantum Noise* (Springer, 2004).
 - [8] J. Kasprzak, M. Richard, S. Kundermann, A. Baas, P. Jeambrun, J. M. J. Keeling, F. M. Marchetti, M. H. Szymańska, R. André, J. L. Staehli, V. Savona, P. B. Littlewood, B. Deveaud and L. S. Dang, Nature **443**, 403 (2006).
 - [9] R. Balili, V. Hartwell, D. Snoke, L. Pfeiffer and K. West, Science **316**, 1007 (2007).
 - [10] D. Bajoni, P. Senellart, E. Wertz, I. Sagnes, A. Miard, A. Lemaître and J. Bloch, Phys. Rev. Lett. **100**, 047401 (2008).
 - [11] J. Klaers, F. Vewinger, M. Weitz, Nat. Phys. **6**, 512 (2010).
 - [12] J. Klaers, J. Schmitt, F. Vewinger, M. Weitz, Nature **468**, 545 (2010).
 - [13] S. Kena-Cohen and S. R. Forrest, Nat. Photon. **4**, 371 (2010).
 - [14] J. D. Plumhof, T. Stöferle, L. Mai, U. Scherf, R. F. Mahrt, Nat. Mat. **13**, 247 (2014).
 - [15] J. Schmitt, T. Damm, D. Dung, F. Vewinger, J. Klaers, M. Weitz, Phys. Rev. A **92**, 011602 (2015).
 - [16] D. Porras, C. Ciuti, J. J. Baumberg and C. Tejedor, Phys. Rev. B **66**, 085304 (2002).
 - [17] G. Malpuech, A. Kavokin, A. Di Carlo, and J. J. Baumberg, Phys. Rev. B **65**, 153310 (2002).
 - [18] M. Maragkou, A. J. D. Grundy, T. Ostatnický and P. G. Lagoudakis, Appl. Phys. Lett. **97**, 111110 (2010).
 - [19] I. Carusotto, M. Wouters, Phys. Rev. B **74**, 245316 (2006).
 - [20] A. Chiochetta and I. Carusotto, EPL **102**, 67007 (2013).
 - [21] A. Chiochetta and I. Carusotto, Phys. Rev. A **90**, 023633 (2014).
 - [22] P. Kirton, J. Keeling, Phys. Rev. Lett. **111**, 100404 (2013).
 - [23] P. Kirton and J. Keeling, Phys. Rev. A **91**, 033826 (2015).
 - [24] C. Aron, G. Biroli, L. F. Cugliandolo, J. Stat. Mech. **2010**, P11018 (2010).
 - [25] L. M. Sieberer, A. Chiochetta, A. Gambassi, U. C. Täuber, and S. Diehl, Phys. Rev. B **92**, 134307 (2015).
 - [26] L. M. Sieberer, S. D. Huber, E. Altman, S. Diehl, Phys. Rev. Lett. **110**, 195301 (2013).
 - [27] L. M. Sieberer, S. D. Huber, E. Altman, S. Diehl, Phys. Rev. B **89**, 134310 (2014).
 - [28] E. G. Dalla Torre, E. Demler, T. Giamarchi and E. Altman, Nat. Phys. **6**, 806 (2010).
 - [29] E. Altman, L. M. Sieberer, L. Chen, S. Diehl, J. Toner, Phys. Rev. X **5**, 011017 (2015).
 - [30] G. Wachtel, L. M. Sieberer, E. Altman, S. Diehl and J. Toner, Phys. Rev. B **94**, 104520 (2016).
 - [31] L. He, L. M. Sieberer, E. Altman, S. Diehl, Phys. Rev. B **92**, 155307 (2015).
 - [32] A. Chiochetta, A. Gambassi, I. Carusotto, arXiv:1503.02816.
 - [33] J. Lebreuilly, I. Carusotto, M. Wouters C. R. Phys. **17** (8), 836 (2016).
 - [34] E. H. Kennard, Phys. Rev. **11**, 29 (1918).
 - [35] B. I. Stepanov, Soviet Phys. - Doklady **2**, 81 (1957).
 - [36] A. Shabani and H. Neven, Phys. Rev. A **94**, 052301 (2016).
 - [37] J. Lebreuilly, A. Biella, F. Storme, D. Rossini, R. Fazio, C. Ciuti, I. Carusotto, Phys. Rev. A **96**, 033828 (2017).
 - [38] G. Guarneri, A. Smirne and B. Vacchini, Phys. Rev. A **90**, 022110 (2014).
 - [39] R. Kubo, Rep. Prog. Phys. **29**, 255 (1966).
 - [40] M. O. Scully and M. S. Zubairy, *Quantum Optics*, Cambridge University Press, (1997).
 - [41] L. Mandel and E. Wolf, *Optical coherence and quantum optics*. Cambridge University Press (1995).
 - [42] L. Pitaevskii and S. Stringari, *Bose-Einstein Condensation*, Oxford University Press (2003).
 - [43] C. Mora and Y. Castin, Phys. Rev. A, **67**, 053615 (2003).
 - [44] K. Iga, IEEE J. Sel. Top. Quantum Electron., **6**(6), 1201 (2000).
 - [45] M. H. Szymanska, J. Keeling, and P. B. Littlewood, Phys. Rev. Lett. **96**, 230602 (2006).
 - [46] M. Wouters and I. Carusotto, Phys. Rev. Lett. **99**, 140402 (2007).
 - [47] G. Grynberg, A. Aspect, and C. Fabre, *Introduction to quantum optics*, Cambridge University press (2010).
 - [48] R. Kubo, J. Phys. Soc. Jpn. **12**(6), 570 (1957).
 - [49] P. C. Martin and J. Schwinger, Phys. Rev. **115**, 1342 (1959).
 - [50] L. F. Cugliandolo, J. Phys. A: Math. Theor., J. Stat. Mech., **44**:483001 (2011).
 - [51] L. Foini, A. Gambassi and L. F. Cugliandolo, P09011 (2012).
 - [52] K. Ji, Kai, V. N. Gladilin and M. Wouters, Phys. Rev. B **91**, 045301, 2015.
 - [53] Those are not actual singularities for a finite dissipation, while the resonance gets sharper and sharper in the weak dissipation limit